

# The US/UK World Magnetic Model for 2005-2010

Susan McLean  
Stefan Maus  
David Dater  
NOAA National Geophysical  
Data Center  
325 Broadway  
NOAA EGC/2  
Boulder, CO 80305-3328  
USA

Susan Macmillan  
Vincent Lesur  
Alan Thomson  
British Geological Survey  
Geomagnetism Group  
Murchison House  
West Mains Road  
Edinburgh EH9 3LA  
UK

Bibliographic Reference:

McLean, S., S. Macmillan, S. Maus, V. Lesur, A. Thomson, and D. Dater, December 2004, *The US/UK World Magnetic Model for 2005-2010*, NOAA Technical Report NESDIS/NGDC-1.



**British  
Geological Survey**  
NATURAL ENVIRONMENT RESEARCH COUNCIL





## **Abstract**

This report contains a detailed summary of the data used, the modeling techniques employed, and the results obtained in the production of the World Magnetic Model (WMM) 2005. This model, valid until 2010.0, is designed for use in air and sea navigation systems. The WMM is a model of the Earth's main magnetic field, that portion of the field generated in the Earth's core.

The World Magnetic Model is a product of the United States National Geospatial-Intelligence Agency (NGA). The U.S. National Geophysical Data Center (NGDC) and the British Geological Survey (BGS) produced the WMM with funding provided by NGA in the USA and by the Defence Geographic Imagery and Intelligence Agency (DGIA) in the UK. The World Magnetic Model is the standard model of the US Department of Defense, the UK Ministry of Defence, the North Atlantic Treaty Organization (NATO), and the World Hydrographic Office (WHO) navigation and attitude/heading referencing systems. It is also used widely in civilian navigation systems.



Abstract.....	i
1. Introduction .....	1
2. Data acquisition and quality control.....	6
2.1. Satellite data .....	6
2.1.1. Ørsted .....	6
2.1.2. CHAMP.....	8
2.1.3. SAC-C .....	13
2.2. Observatory data.....	14
3. Data selection for WMM2005.....	17
3.1. Selection and pre-processing for parent model .....	18
3.2. Selection to enable forward prediction to 2010.0.....	19
4. Modeling methods.....	25
4.1. Model parameterization.....	25
4.2. Model determination .....	28
4.3. Coordinate transformation.....	29
4.4. Secular variation prediction.....	31
4.5. Data weighting schemes .....	31
4.6. Derivation of WMM2005.....	32
5. Resulting model.....	33
5.1. Model coefficients .....	33
5.2. Magnetic pole and eccentric dipole locations .....	36
5.3. Equations for computing the magnetic field elements .....	36
5.4. Model accuracy .....	39
5.5. Model limitations.....	44
6. Test values .....	45
7. Contacts .....	46
Acknowledgements .....	47
Maps .....	48
Main field maps: Mercator Projection.....	48
Main field maps: North Polar Stereographic Projection .....	52
Main field maps: South Polar Stereographic Projection .....	55
Secular variation maps: Mercator Projection .....	59
Secular variation maps: North Polar Stereographic Projection.....	62
Secular variation maps: South Polar Stereographic Projection.....	66
References .....	69

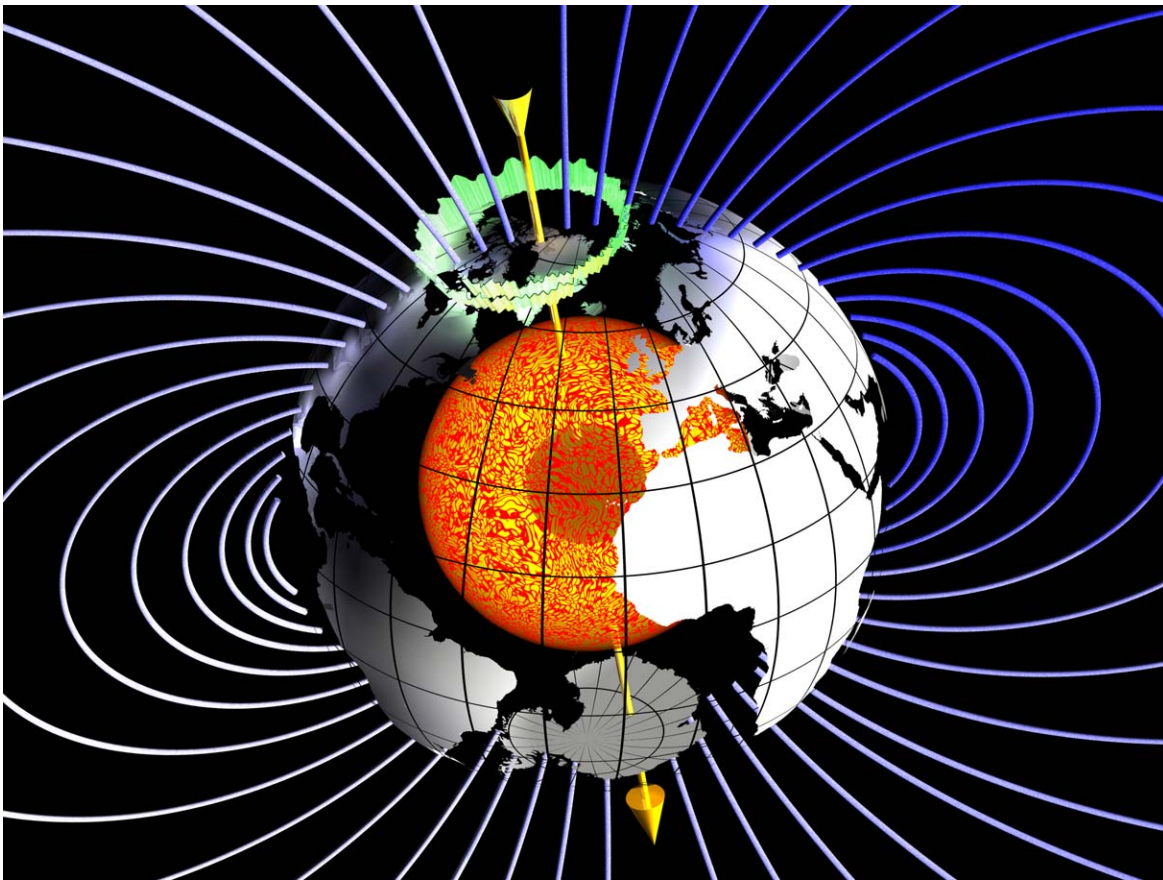


## 1. Introduction

The Earth's magnetic field ( $\mathbf{B}$ ) is a vector quantity varying in space ( $\mathbf{r}$ ) and time ( $t$ ). The field, as measured by a magnetic sensor on or above the Earth's surface, is actually a composite of several magnetic fields, generated by a variety of sources. These fields are superimposed on each other and through inductive processes interact with each other. The most important of these geomagnetic sources are:

- a. the main field (Figure 1), generated in Earth's conducting, fluid outer core ( $\mathbf{B}_m$ );
- b. the crustal field from Earth's crust/upper mantle ( $\mathbf{B}_c$ );
- c. the combined disturbance field from electrical currents flowing in the upper atmosphere and magnetosphere, which also induce electrical currents in the sea and the ground ( $\mathbf{B}_d$ )

**Figure 1: The main magnetic field generated by dynamo action in the hot, liquid outer core. Above Earth's surface, nearly dipolar field lines are oriented outwards in the southern and inwards in the northern hemisphere (courtesy Martin Rother GFZ, Potsdam)**



Thus, the observed magnetic field is a sum of contributions

$$\mathbf{B}(\mathbf{r}, t) = \mathbf{B}_m(\mathbf{r}, t) + \mathbf{B}_c(\mathbf{r}) + \mathbf{B}_d(\mathbf{r}, t) \quad (1)$$

$\mathbf{B}_m$  is the dominating part of the field, accounting for over 95% of the field strength at the Earth's surface. *Secular variation* is the slow change in time of  $\mathbf{B}_m$ .  $\mathbf{B}_c$ , the field arising from magnetized crustal rocks, varies spatially, but is considered constant in time for the time-scales considered here.  $\mathbf{B}_c$  is usually much smaller in magnitude than  $\mathbf{B}_m$ . The crustal field is constant over the time-scales considered here. The field arising from currents flowing in the ionosphere and magnetosphere and their resultant induced currents in the Earth's mantle and crust,  $\mathbf{B}_d$ , varies both with location and time. The WMM represents only the main geomagnetic field,  $\mathbf{B}_m$ .

To create an accurate main field model, it is necessary to have data with good global coverage and as low a noise level as possible. The Danish Ørsted and German CHAMP satellite data sets satisfy these requirements. Both satellites provide high quality vector and scalar data at all latitudes and longitudes, but not during all time periods needed for modeling. These satellite data were therefore augmented with ground observatory hourly mean data, which were available almost continuously over the period of interest, although with poorer spatial coverage. The observatory data therefore provide valuable constraints on the time variations of the geomagnetic field. Used together, satellite and observatory data provide an exceptional quality data set for modeling the behaviour of the main magnetic field in space and time.

$\mathbf{B}_c$  has spatial variations on the order of meters to thousands of kilometers and cannot be fully modeled with low degree spherical harmonic models. Therefore, the WMM does not include contributions from the crust except for those of very long wavelength.  $\mathbf{B}_c$  is usually smaller at sea than on land, and decreases with increasing altitude. The rock magnetization resulting in  $\mathbf{B}_c$  may be either induced (by the main magnetic field) or remnant or a combination of both.

The field arising from currents flowing in the ionosphere and magnetosphere and their associated induced currents in the Earth,  $\mathbf{B}_d$ , varies both with location and time. Figure 2 shows the various current systems. The disturbance field can vary both regularly, with fundamental periods of one day and one year, as well as irregularly on time scales of seconds to days. The regular variations are both diurnal and annual and they are essentially generated by the daylight

atmosphere at altitudes of 100-130 km, ionized by the Sun's radiation, being moved in the Earth's main field by winds and tides, thus producing the necessary conditions (motion of a conductor in a magnetic field) for a dynamo to operate. Further daily and annual variations are caused by the rotation of the Earth in the external magnetospheric field, which is organized in a sun-synchronous reference frame. The irregular variations are due to magnetic storms and sub-storms. Magnetic storms generally have three phases: an initial phase, often with a sudden commencement and increased horizontal field at mid-latitudes, a main phase, and a recovery phase. The main phase involves an intensification of the ring current (Figure 2) from the plasma sheet.

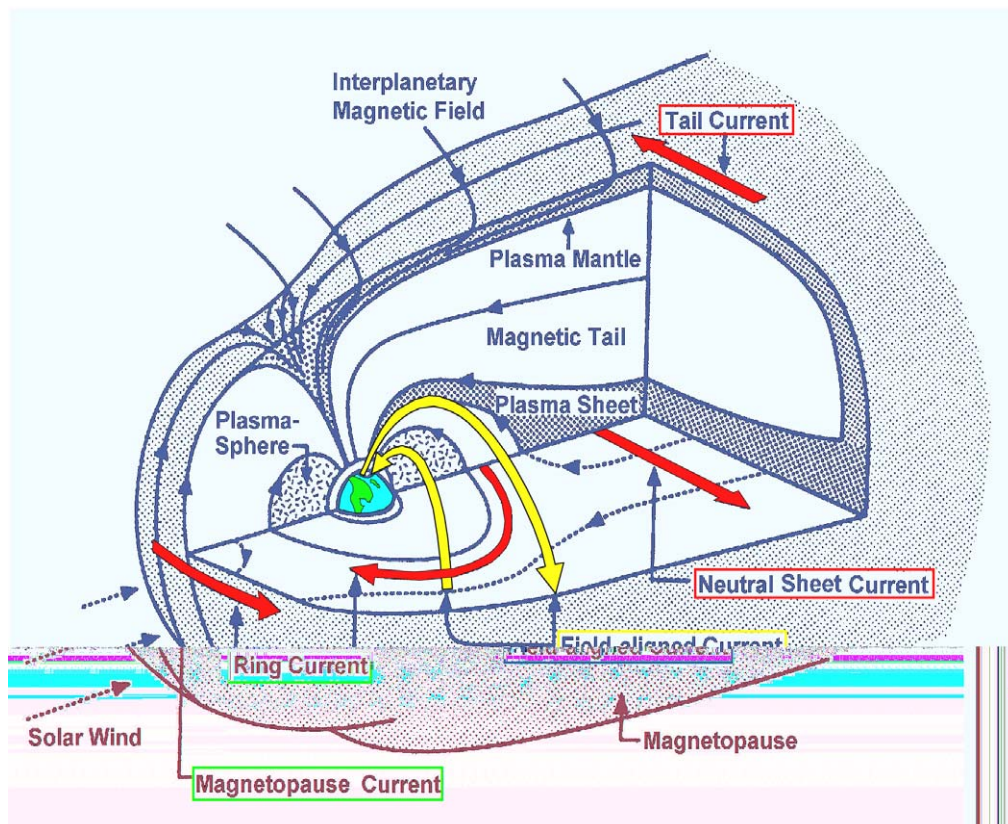


**Figure 2: Magnetospheric current systems (red) generate a magnetic field, which is almost uniform, close to the earth. Field-aligned currents (yellow) couple the**

During the recovery phase the ring current returns to normal over a number of days and associated sub-storms subside. Magnetic storm and sub-storm effects are generally more severe at high geomagnetic latitudes where the ionized region of the upper atmosphere (the ionosphere) is coupled to the magnetosphere by field-aligned currents and is therefore strongly

influenced by the interplanetary magnetic field and current systems in the magnetotail. Both the regular and irregular disturbance field variations are modulated by season and the solar magnetic activity cycle. The primary disturbance field is often known as the external field, as its main sources, the ionosphere and magnetosphere, are external to the surface of the Earth where geomagnetic measurements were traditionally made. However, this term can be confusing and is avoided when using satellite data, as the ionosphere is below the altitude of these data and is therefore effectively internal to this observation surface. For further information about the crustal and disturbance fields (and general information about geomagnetism) see Merrill et al. (1996) and Parkinson (1983).

The geomagnetic field vector,  $\mathbf{B}$ , is described by 7 elements. These are: the orthogonal components  $X$  (northerly intensity),  $Y$  (easterly intensity), and  $Z$  (vertical intensity, positive downwards), total intensity  $F$ , horizontal intensity  $H$ , inclination (or dip)  $I$  (the angle between the horizontal plane and the field vector, measured positive downwards), and declination (or magnetic variation)  $D$  (the horizontal angle between true north and the field vector, measured positive eastwards). Declination, inclination, total intensity, and GV, the grid variation, can be computed from the orthogonal components using the equations:

$$\begin{aligned}
 H &= \sqrt{X^2 + Y^2}, & F &= \sqrt{H^2 + Z^2}, & D &= \arctan(Y, X), & I &= \arctan(Z, H), \\
 GV &= D - \lambda \quad \text{for } \varphi > 55^\circ, & GV &= D + \lambda \quad \text{for } \varphi < -55^\circ
 \end{aligned}
 \tag{2}$$

where  $\arctan(a, b)$  is  $\tan^{-1}(a/b)$ , taking into account the angular quadrant, avoiding a division by zero, and resulting in a declination in the range of  $-180^\circ$  to  $180^\circ$  and inclination of  $-90^\circ$  to  $90^\circ$ . For  $H=0$  the declination is undefined. The vector components are observed in the geodetic, i.e. ellipsoidal, coordinate system as well as in spherical geocentric coordinates. In the latter case a prime is added, as in  $X'$ ,  $Y'$  and  $Z'$ . Table 1 shows the expected range of values for the magnetic components and GV at Earth's surface.

**Table 1: Range of magnetic elements and GV at the Earth's surface.**

			Range at Earth surface		
Element	Name	Alternative name	Min	Max	Unit
<b>X</b>	North component	Northerly intensity	-17,000	42,000	nT
<b>Y</b>	East component	Easterly intensity	-18,000	18,000	nT
<b>Z</b>	Down component	Vertical intensity	-67,000	61,000	nT
<b>H</b>	Horizontal Intensity		0	42,000	nT
<b>F</b>	Total Intensity	Total field	22,000	67,000	nT
<b>I</b>	Inclination	Dip	-90	90	degree
<b>D</b>	Declination	Magnetic variation	-180	180	degree
<b>GV</b>	Grid variation	Grid Magnetic Variation	-180	180	degree

The WMM for 2005 – 2010 comprises a degree and order 12 spherical-harmonic main field model for 2005.0, and a degree and order 8 spherical-harmonic predictive secular variation model for the period 2005.0 to 2010.0. WMM2005 supersedes WMM2000 (Quinn and Macmillan, 1999; Macmillan and Quinn, 2000) and should replace this model in navigation systems. Also included with the model is computer software for computing the magnetic field components *X*, *Y*, *Z*, *F*, *D*, *I*, and *H* in geodetic coordinates. The current WMM will be replaced with a new degree and order 12 main field and predictive secular-variation model in 2010.

The model, associated software, digital charts, and documentation are available by contacting NGDC, BGS, or NGA at the addresses listed in Section 7, or via the Web at <http://www.ngdc.noaa.gov/seg/WMM/>. The military specifications for the WMM are contained in MIL-W-89500 (Defense Mapping Agency, 1993). Magnetic model requirements that are more stringent than those set forth in this military specification (e.g., those which must include magnetic effects of the Earth's crust, ionosphere, or magnetosphere and/or require greater spatial or temporal resolution on a regional or local basis) should be addressed to NGA.

## 2. Data acquisition and quality control

### 2.1. Satellite data

The principal characteristic of satellite data is their global coverage often obtained within a relatively short time span. The inclination of the orbit (the angle between the plane containing the satellite's path and the Earth's equatorial plane) determines the latitudinal extent of the data coverage; an inclination of  $90^\circ$  provides 100% coverage, an inclination of slightly less or slightly more than  $90^\circ$  results in gaps with no data for small regions around the geographic poles. Another important characteristic of satellite data is that the crustal field is strongly attenuated due to the distance of the satellite from the Earth's crust.

A high inclination satellite is more or less stationary in local time, with the Earth rotating beneath it. Thus, it provides a crude picture of the Earth within 24 hours. During this time it completes about 15 orbits, with a longitudinal spacing of around 24 degrees. One drawback of this sun-synchronous orbit is that all night-side observations at a given latitude have nearly the same local time for an extended period of time. Consequently, modeling external fields that are dependent on local time can be difficult from such data. The Magsat satellite, which made an accurate vector magnetic survey for 7 months in the winter of 1979/1980, is an example of a strictly sun-synchronous orbit with dawn and dusk being the local times sampled (Langel and Hinze, 1998). Similarly, the satellite SAC-C is on a fixed noon/midnight orbit, while Ørsted and CHAMP slowly drift in local time (details below). The local time drift depends on the orbit inclination, which is usually chosen in such a way to avoid multiples of annual frequencies, in order to be able to separate annual and local time dependent contributions to the external magnetic field. Because the connection between the star imager and the vector magnetometer on SAC-C is defective, only Ørsted and CHAMP data have been used in the production of WMM2005.

#### 2.1.1. Ørsted

The Danish satellite Ørsted is a dedicated satellite for geomagnetic field modeling. It was successfully launched on 23 February 1999 from Vandenberg Air Force Base in California on a Delta II rocket, along with the American ARGOS (Advanced Research Global Observation

Satellite) and the South African micro-satellite SUNSAT. Initially planned for a minimum of 14 months, as of October 2004 Ørsted is still delivering high quality data. The Ørsted website is at <http://web.dmi.dk/fsweb/projects/oersted/>.

### Satellite and Orbit

The Ørsted satellite (Figure 3) has a mass of 62 kg and measures 34x45x72 cm when the 8-m boom is stowed. The main receiving station is at the Danish Meteorological Institute (DMI) in Copenhagen. The satellite was launched into a retrograde orbit with the ascending node at start of mission being 14:11 local time, apogee ~850 km, perigee ~640 km, inclination 96.5°, nodal period 99.6 minutes, longitude increment -24.9°/orbit and local time increment -0.88 minutes/day, corresponding to a drift of the orbital plane by 128.5°/year. The satellite velocity is approximately 7.5 km/second.

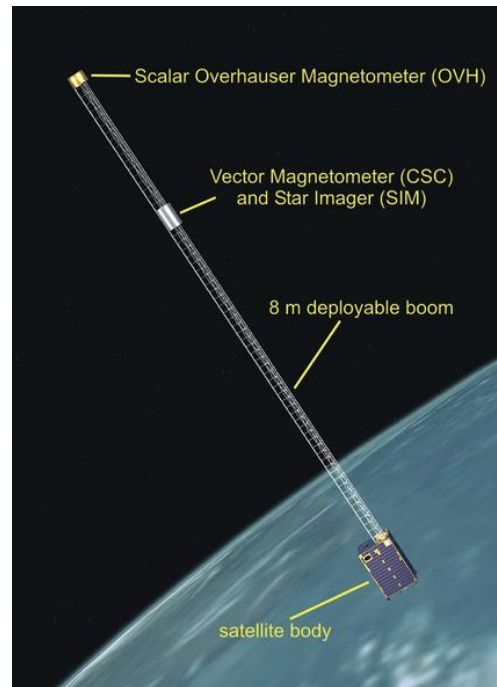


**Figure 3: Ørsted satellite**

### Magnetometers

At the quietest location, the tip of the 8 m boom, an Overhauser magnetometer (OVM) measures the strength of the magnetic field (not direction sensitive). It is accurate to 0.5 nT. The main purpose of this instrument is the absolute calibration of the measurements of the Compact Spherical Coil (CSC) instrument. It was built at the French Electronic Technology Laboratory, LETI, and was provided by the French Space Agency, CNES. At some distance from the OVM (to avoid mutual disturbances of the magnetometers), a CSC fluxgate magnetometer measures the magnetic vector field (strength and direction). This instrument is stable within 0.5 nT over time spans of several days. It was built at the Danish Technical University (DTU).

### Star Imager

A single head star-imager is co-located with the CSC-magnetometer to determine its orientation. The star imager is accurate to about 30 arc-seconds for rotations around its axis of

vision (bore sight) and to about 5 arc-seconds for rotations about any axis perpendicular to the bore sight. This instrument was built at the DTU.

#### Particle Detectors

Particle detectors were placed on the main body of the satellite to measure the flux of high energy electrons (0.03-1 MeV), protons (0.2-30 MeV), and alpha-particles (1-100 MeV) around the satellite. These instruments were built at the Danish Meteorological Institute.

#### Global Positioning System (GPS) Receivers

Ørsted has a Turbo-Rogue GPS Receiver to accurately determine the position of the satellite and provide time synchronization for the instruments. The GPS Receiver was supplied by NASA, and was built at their Jet Propulsion Laboratory (JPL).

#### Data Products

The calibrated data products relevant to main field modeling are the 'MAG-F' product for the strength of the field (scalar data) and the 'MAG-L' product for the vector field. The data are archived and distributed by the Ørsted Science Data Center at

<http://dmiweb.dmi.dk/fsweb/projects/oersted/SDC>.

#### 2.1.2. CHAMP

The CHAllenging Minisatellite Payload (CHAMP) is a German satellite mission dedicated to improving gravity and magnetic field models of the Earth. CHAMP was proposed in 1994 by Christoph Reigber of GeoForschungsZentrum Potsdam in response to an initiative of the German Space Agency (DLR) to support the space industry in the "New States" of the united Germany. Hermann Lühr leads the magnetic part of the mission. CHAMP was launched with a Russian COSMOS vehicle on 15 July 2000 into a low Earth orbit. Initially planned to last 5 years, the mission is now projected to extend to 2008. The official CHAMP website is at

<http://op.gfz-potsdam.de/champ/>.

#### Satellite and Orbit

A limiting factor for low Earth satellite missions is the considerable drag of the atmospheric neutral gas below 600 km altitude. Satellite drag was the primary factor in the short lifespan (7 months) of Magsat and the choice of a higher altitude orbit for Ørsted. To achieve long mission

duration on a low orbit, CHAMP was given high weight (522 kg), a small cross section, and a stable attitude. It was launched into an almost circular, near polar (inclination = 87.3°) orbit with an initial altitude of 454 km. While Magsat was on a strictly sun-synchronous dawn/dusk orbit, CHAMP advances one hour in local time within eleven days. It takes approximately 90 minutes to complete one revolution at a speed of about 8 km/s. The decay of CHAMP's orbital altitude depends on the neutral gas density, which is enhanced by solar activity. CHAMP's orbit has been raised twice to prolong the mission (Figure 4).

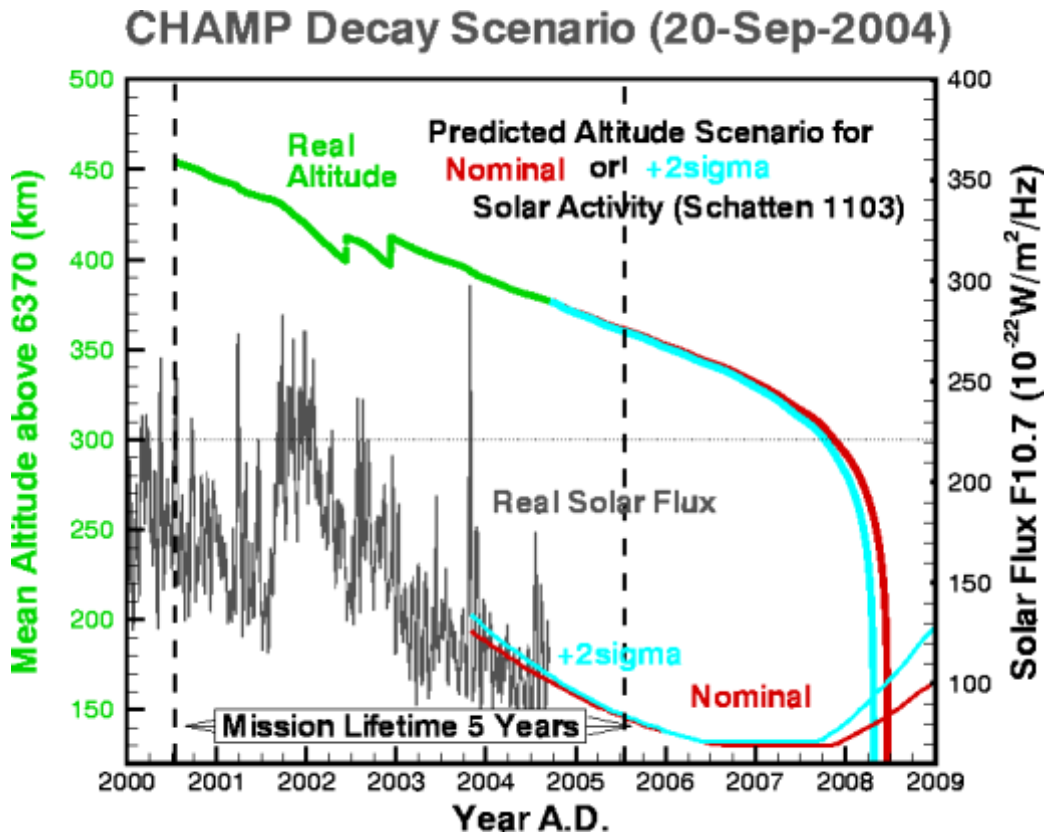


Figure 4: The decay of CHAMP's orbital altitude.

Magnetic Mission Instrumentation

The magnetic instruments of CHAMP are very similar to those of Ørsted. CHAMP carries the same scalar and vector magnetometers. The star imager is built by the same laboratory, but is equipped with a dual head (Figure 5).

## Magnetometers

At the tip of the 4 m long boom, a proton precession Overhauser magnetometer measures the total intensity of the magnetic field, once per second. This instrument, which was developed by LETI has an absolute accuracy of 0.5 nT. Its measurements are used in the absolute calibration of two redundant vector magnetometers, located mid-boom on an optical bench. These fluxgate magnetometers were developed and supplied by DTU. They sample the field at 50 Hz with a resolution  $< 0.1$  nT.

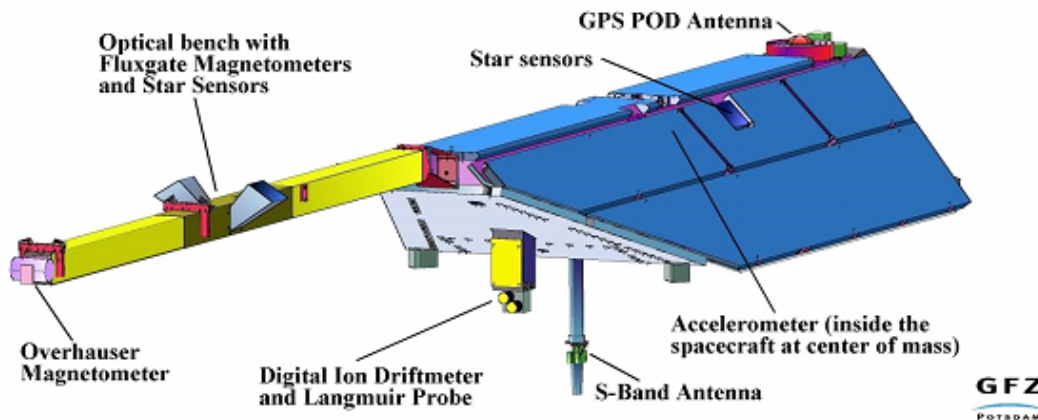


**Figure 5: Front view of the CHAMP satellite.**

## Star Imagers

A star imager, developed and supplied by DTU, gives the orientation of the optical bench in space. Attitude uncertainty is the largest source of error in satellite vector magnetic data. Star imagers are often blinded by the sun or moon and provide unreliable attitude with regard to rotations about their direction of vision (bore sight). For this reason, CHAMP was equipped with a dual head star imager, improving relative attitude by an order of magnitude to about 3-arc seconds accuracy for rotations about all axes, corresponding to around 0.5 nT accuracy for the vector components. Since this high accuracy is only achieved in dual head mode (available for 62% of CHAMP data), future magnetic field missions (e.g. the European Space Agency mission *Swarm*, scheduled for launch in 2009) will have triple head star imagers. A further, redundant dual head star imager on the body of CHAMP is of limited utility for the magnetic field measurements, due to the flexibility of the boom.

### Electric Field, Electron Density and Temperature

The U.S. Air Force Research Laboratory provided a Digital Ion Drift Meter (DIDM) and a Planar Langmuir Probe (PLP). The DIDM, designed to measure the electric field from ion velocities, partly failed due to frictional overheating during the launch phase of CHAMP. The PLP, which was not damaged, provides the spacecraft potential, electron temperature and electron density, once every 15 seconds. These quantities are used to correct magnetic field measurements for the diamagnetic effect of the plasma surrounding the satellite. The PLP measurements have turned out to be very useful for accurate geomagnetic field modeling.

### GPS Receiver

Apart from providing the accurate position of CHAMP, the Black Jack GPS receiver (supplied by NASA) has the important task of providing an absolute time frame. A pulse delivered every second is used to synchronize all of the instruments on board. Furthermore, it provides a stable reference frequency for the proton precession magnetometer readings, giving them absolute accuracy.

### Data Products

CHAMP's standard science products are labeled from level-0 to level-4, according to the amount of pre-processing applied to the original data. Scientific utility starts with level-2 products, which are calibrated, flagged and merged with accurate orbits and are supplied as daily files in Common Data Format (CDF). Level-3 products comprise the final processed, edited, and calibrated data, as well as the rapid delivery products. As of October 2004, final level-3 data for the magnetic field are still not available, due to problems with the absolute calibration of the star sensor. An attitude correction therefore had to be applied to the CHAMP level-2 data before use in the WMM. The correction is described in a separate section, below. The level-2 to level-4 products are archived and distributed by the Information System and Data Centre (ISDC) at GFZ Potsdam (<http://isdc.gfz-potsdam.de/champ/>).

### CHAMP Star Imager Calibration

An important step in pre-processing vector satellite magnetic measurements is the calibration of the alignment between the internal coordinate system of the vector magnetometer and the internal coordinate system of the star imager. Since these coordinate systems experience small (but significant) changes in their orientation against each other, a regularly updated calibration

is essential. This calibration has been carried out for Magsat and Ørsted data, but not for the present CHAMP level-2 data. The final level-3 data will be fully corrected for this effect.

As a preliminary calibration, we have estimated a continuous time series of the misalignment angles. A 3-day window was moved over the CHAMP vector data set. From the night-side data in the range of  $-60^\circ$  to  $+60^\circ$  latitude three misalignment correction angles were estimated by minimizing the root mean square (RMS) of the vector component residuals. The procedure is robust because constant misalignments have signatures that are distinctly different from those of genuine magnetic fields.

Once the time series of misalignment angles has been estimated, a simple point-by-point correction can be applied to all CHAMP vector data. The calibration file, a C-language procedure callable from FORTRAN, and a Matlab interface are available at <http://www.gfz-potsdam.de/pb2/pb23/SatMag/sca.html>

Applying the correction significantly reduces the residuals of CHAMP vector data. Table 1 shows the RMS difference between data and a field model for pre- and post-calibrated data, and comparing these with the RMS of Ørsted data. Considering that higher residuals are expected for CHAMP data, due to its closer proximity to crustal and ionospheric sources (as manifested in  $F$ ), the correction reduces CHAMP vector residuals to well below Ørsted levels. Thus, the correction realizes the full potential of the low attitude noise of CHAMP's dual head star imager.

**Table 2: The RMS of residuals for all available quiet nighttime data (0-4 LT,  $K_p < 2$ ,  $Dst < 20$ , CHAMP single and dual-head modes) of 2000-2004, against the model Oersted-04i-04 (Olsen, 2004). This model is partly based on CHAMP scalar data, but not on CHAMP vector data.**

	Ørsted	CHAMP pre-cal	CHAMP post-cal
	RMS	RMS	RMS
$X$	7.9	13.5	6.2
$Y$	7.0	9.9	5.0
$Z$	5.4	9.6	4.7
$F$	3.5	3.9	3.9

### 2.1.3. SAC-C

Argentina's SAC-C spacecraft was designed to study the structure and dynamics of the Earth's atmosphere, the ionosphere, and the geomagnetic field. A Delta-2 vehicle successfully launched SAC-C, together with satellites EO-1 and Munin, from Vandenberg Air Force Base on 21 November 2000. The spacecraft weighs approximately 475 kg with a size at launch configuration of 2.1 x 1.9 x 1.7 m (Figure 6). NASA provided the launch vehicle and some science instruments and NASA's Goddard Space Flight Center, Greenbelt, Maryland, is responsible for overall project management. The Danish Space Research Institute provided the magnetic instrumentation, including the 8 m extendable boom. The vector magnetometer and star imager are very similar to those



**Figure 6: Artist's impression of SAC-C in orbit.**

on Ørsted, but NASA's JPL built and supplied the Scalar Helium Magnetometer (SHM). As

with Ørsted, the scalar magnetometer is mounted at the tip of the extendable boom.

Unfortunately, the connection between the star imager and the vector magnetometer turned out to be defective after launch. The scalar magnetometer provides the only useable data. This scalar data has a good relative accuracy of a few nT. In order to be used for main field modeling, though, the data would have to be calibrated to absolute accuracy. This would not be difficult and could be achieved using field models from Ørsted and CHAMP. However, as of October 2004, such a calibration had not been undertaken. The data would actually be very useful, since SAC-C is on a fixed local time orbit, complementing the drifting orbits of Ørsted and CHAMP. Due to the lack of absolute calibration, SAC-C data could not be used for the WMM2005. The SAC-C website is at <http://orbis.conae.gov.ar/sac-c/>.

## 2.2. Observatory data

One of the principal characteristics of observatory data is the long-term continuous coverage in time in the region where the WMM is most used. This means that prediction of the magnetic field for several years into the future, as required by the WMM, is possible and that the regular and irregular variations in the external field can be characterized and their effects minimized in the WMM. The spatial distribution of observatories is largely determined by the location of habitable land and by the availability of local expertise, funds, and energy supply, and while it is uneven and a little sparse in some regions, it has been reasonably constant in time (Figure 7).

### Instrumentation

There are three categories of instruments at an observatory. The first category comprises variometers, which make continuous measurements of elements of the geomagnetic field vector. Both analogue and digital variometers require temperature-controlled environments, extremely stable platforms, and can generally operate without manual intervention. The most common type of variometer today is the tri-axial fluxgate magnetometer.

The second category comprises absolute instruments that can make measurements of the magnetic field in terms of absolute physical basic units or universal physical constants. The most common types of absolute instrument are the fluxgate theodolite, for measuring  $D$  and  $I$ , and the proton precession magnetometer for measuring  $F$ . In the former instrument the basic unit of measurement is an angle. To determine these angles the fluxgate sensor mounted on the telescope of a non-magnetic theodolite is used to detect when it is perpendicular to the magnetic field vector. With the fluxgate sensor operating in this null-field mode, the stability of the sensor and its electronics is maximized. To complete the determination of  $D$  and  $I$ , true north is found by reference to a fixed mark of known azimuth, usually determined by astronomical observations. In a proton precession absolute magnetometer, the universal physical constant is the gyromagnetic ratio of the proton. Measurements with a fluxgate theodolite can only be made manually while a proton magnetometer can operate automatically.

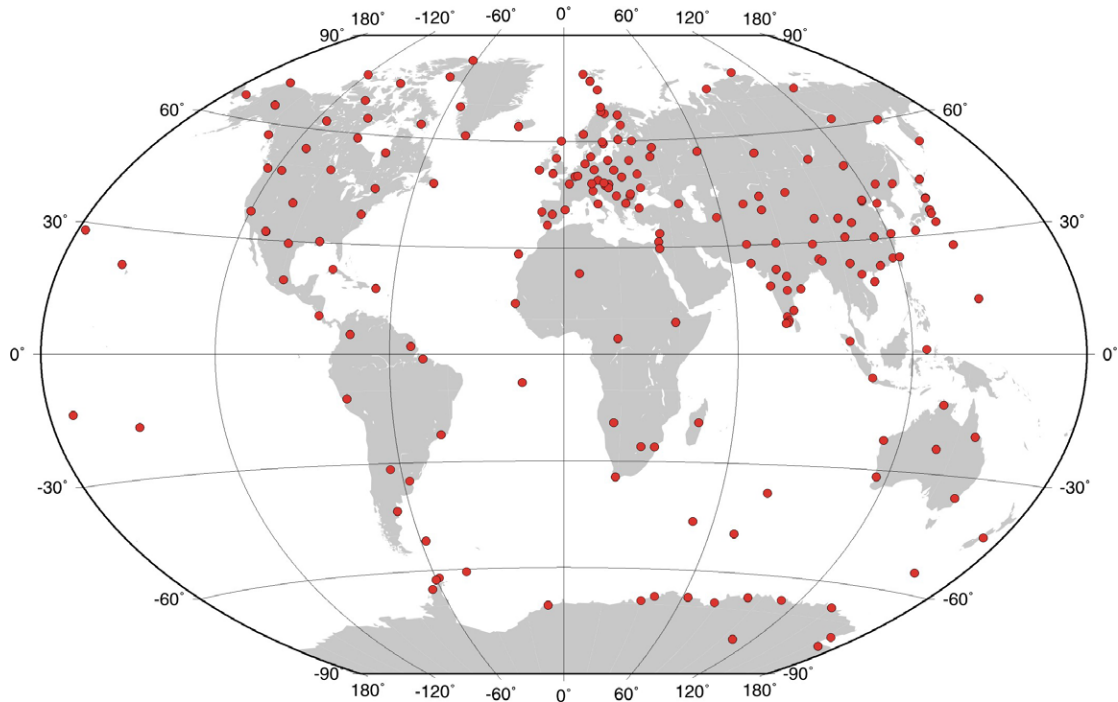


**Figure 7: Locations of all observatories that contributed data to WMM2005**

The third category comprises semi-absolute measurements. These are instruments that measure deviations from a field, which is determined on a regular basis using an absolute instrument. An example is a proton vector magnetometer where artificial orthogonal bias fields are applied to a proton precession magnetometer sensor, located at the center of a set of coils through which currents can be passed, to obtain the components of the field vector. Like variometers, these instruments are temperature-sensitive and require stable platforms. For more information on magnetic instrumentation and operation of magnetic observatories, the reader is referred to Jankowski and Sucksdorff (1996).

#### Data Collation and Quality Control

BGS and NGDC actively collect observatory data through their involvement in the World Data Center system. They maintain databases suitable for magnetic field modeling, maintain contacts with organizations operating magnetic observatories, and collaborate with the other WDCs. Each year BGS sends requests to all organizations operating observatories for the latest data and other relevant information. The WDCs in Edinburgh (BGS) and Boulder (NGDC) assimilate annual mean values. The WDCs in Copenhagen and Boulder assimilate hourly mean

values. The hourly mean values used for the WMM were downloaded from the WDC Copenhagen website at <http://dmiweb.dmi.dk/fsweb/projects/wdccc1>.

BGS also actively collects global observatory data through its involvement in INTERMAGNET. The objectives of INTERMAGNET are to establish a global network of cooperating digital magnetic observatories, to adopt modern standard specifications for measuring and recording equipment, and to facilitate data exchange and the production of geomagnetic products in close to real time. In addition to operating five of the observatories shown in Figure 7, BGS operates one of six INTERMAGNET GINs (Geomagnetic Information Node), and plays a leading role in the INTERMAGNET organization. The INTERMAGNET website is <http://www.intermagnet.org>.

The quality of the data an observatory produces is the responsibility of the operator. The most important aspect of for global modeling is the stability of the baseline. A baseline is the difference between the calibrated variometer data and the absolute observations. A baseline with many points, low scatter, few drifts and offsets is a sign of good quality. Baseline plots for the INTERMAGNET observatories are available on the annual CDs of definitive data.

Quality assurance and control measures, other than those carried out by the observatory operators, are also carried out by INTERMAGNET through its observatory standardization program, the World Data Centers, and by participation of many observatory operators in the International Association of Geomagnetism and Aeronomy (IAGA) Observatory Workshops.

Final quality control procedures, prior to deriving the WMM, are carried out by BGS. For the hourly means, this involves plotting all data to identify typographical errors and jumps, and plotting differences between data and initial global models to identify drifts. If a problem in a particular dataset for the WMM is identified, an enquiry is sent to the observatory operator. If this problem is not resolved, the data are not used in the production of the final WMM.

### 3. Data selection for WMM2005

The WMM models the main field,  $\mathbf{B}_m$ , and its slow variation with time, the ‘secular variation’ for 2005-2010. However, the geomagnetic field as measured on the Earth surface or at satellite altitude is a combination of several magnetic fields. All the other contributions have to be modeled together with the main field or they will be partially mapped into the model residuals, with the risk of introducing biases into the model of  $\mathbf{B}_m$ . Most of the fields generated external to the solid Earth are highly variable in time and prove difficult to accurately model. Our data selection process therefore tries to minimize the contributions of these fields and their induced effects in the solid Earth. There are three main selection criteria:

1. Data are selected only on the night side of the Earth
2. Data are selected only during magnetically quiet periods
3. Only scalar data are selected at high latitudes

The first criterion is very effective in minimizing the contribution from the magnetic field generated in the ionosphere, since ionospheric conductivity is high only on the dayside of the Earth. Magnetically quiet periods are those intervals when the external fields are relatively weak and when they do not vary excessively in time. The identification of quiet periods relies on the Kp and Dst indices (computed from observatory data), from measurements of the Interplanetary Magnetic Field (IMF) strength and direction, and the solar wind speed. Scalar data are selected at high latitudes to minimize the effects of ever-present current systems in these regions, which generate a high level of noise in the vector data.

The planetary Kp ("*p*planetarische Kennziffer") index is based on the K-index, a local index of the 3-hourly range in magnetic activity of the two horizontal field components (X and Y) relative to an assumed quiet-day curve for the geomagnetic observatory. Local disturbance levels are determined by measuring the range (difference between the highest and lowest values) during three-hourly time intervals for the most disturbed magnetic field component. The range is then converted into a local K index according to a pseudo-logarithmic scale, which is station specific. This is an attempt to normalize the frequency of occurrence of the different sizes of disturbances. The three-hourly Kp index (average of local K values from 12 selected,

subauroral stations including Lerwick, Eskdalemuir and Hartland observatories in the UK) is expressed in a scale of thirds (28 values).

Charged particles trapped by the geomagnetic field in the magnetosphere drift around the Earth at a distance of 3-8 Earth radii creating a westward electric ring current whose field opposes the main geomagnetic field. The strength of this field is of the order of tens of nT during quiet times and several hundred nT during magnetic storms. Magnetopause, tail, and partial ring currents make additional contributions leading to asymmetries in the field which increase during storms. The symmetric part of this composite disturbance field is tracked by the Dst (disturbance storm-time) index (Sugiura, 1964), derived from the measurements of four low latitude observatories.

In deriving the WMM, the main field and the secular variation are modeled together and then modeled again separately for the predictive component. This strategy means that different data can be used for main-field and predictive secular-variation modeling, thereby optimizing their different qualities. As the WMM is intended for navigation, it must accurately compute magnetic field values for the entire 5-year lifespan of the model. The ability to model the secular variation is therefore very important and long-term data from observatories are incorporated at this stage.

### **3.1. Selection and pre-processing for parent model**

In this section we describe the data requirements to produce a main field model valid between 1999.0 and 2004.5. The emphasis is on the availability of data with good global coverage and a noise level as low as possible. The Ørsted and CHAMP satellite data sets satisfy these requirements. CHAMP is the lower of the two satellites and is therefore subject to a higher level of noise. This noise is due to the crustal field signal,  $\mathbf{B}_c$ , (not included in the WMM) and to systems of electrical currents flowing between the Earth's surface and the satellite path, predominantly at high latitude. On the other hand, the CHAMP data acquired at low altitude provide better constraints on the short wavelengths of the internal geomagnetic field model.

Both satellites provide high quality vector and scalar data at all latitudes and longitudes. However, due to the inclination of both satellites' orbits, these data are not always available in the narrow time window used in our data selection process. Gaps are evident in the joint data set during years 2000 and 2002 (Figure 8). By contrast, the observatory hourly mean data set is almost continuous over the whole period of interest, although the spatial coverage is poorer (Figure 8). The observatory data therefore gives good constraints on the time variations of the geomagnetic field. The noise level in the observatory data is higher than in the satellite data, due to the closer proximity of the observatories to conducting bodies in the crust. Time varying external fields induce electrical currents in these conductors, generating magnetic disturbances at the observatories.

CHAMP satellite magnetic measurements are affected by the diamagnetic effect of the ambient plasma (Lühr et al., 2004), which decreases magnetic field readings. The effect is of the order of a few nT and is strongest near the magnetic equator in the pre-midnight hours. Using the electron density and temperature readings from CHAMP's Langmuir probe, a simple diamagnetic correction was applied to the CHAMP data. Due to its higher flight altitude, such a correction was not necessary for Ørsted data.

### **3.2. Selection to enable forward prediction to 2010.0**

Prediction of secular variation to 2010.0 depended partly on long series of observatory annual means in  $X$ ,  $Y$ , and  $Z$ . As the satellite and observatory hourly mean data covers only about 5 years, predictions of up to 6 years into the future, i.e. 2004 and onwards, benefit from the incorporation of data covering a longer interval. Time series from 188 observatories (Figure 7) were selected using the file of annual means maintained by BGS ([www.geomag.bgs.ac.uk/gifs/annual\\_means.shtml](http://www.geomag.bgs.ac.uk/gifs/annual_means.shtml)). This involved subjective selection, based on continuity and length of time series and knowledge of observing practice, and plotting all data to identify unspecified jumps and early parts of records that were noisy. Any known discontinuities, for example resulting from change of location of the absolute observing pillar, were applied. The list of observatories used, and the coverage in time, is given in Table 3.

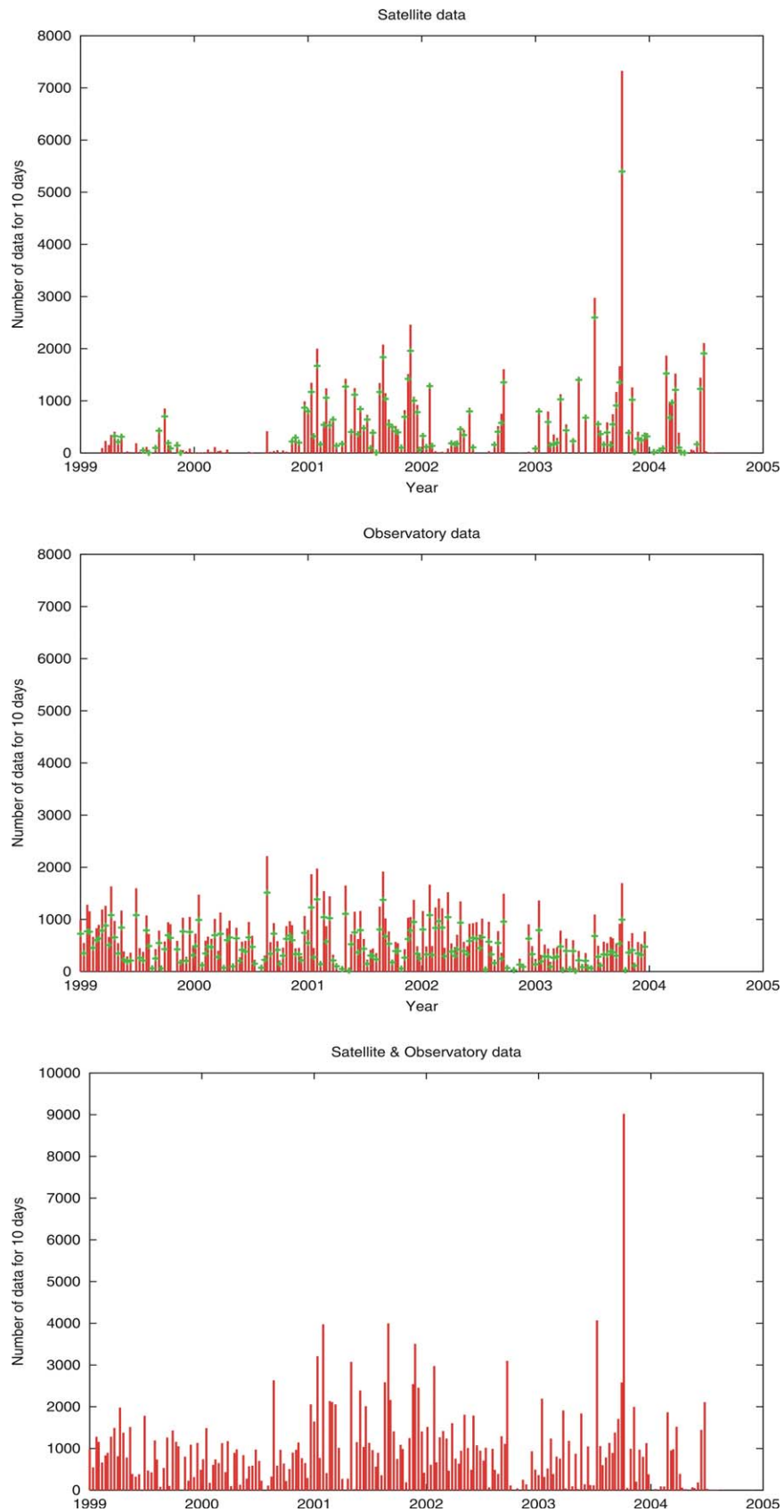


**Figure 8: Distribution of satellite, observatory, and final vector and scalar data in time 1999.0 - 2004.5. Green bars indicate the number of vector data; remaining data are scalar, mainly at high latitudes.**

**Table 3: IAGA code, name, geodetic latitude, and longitude of observatory and data time span used for secular variation prediction.**

Code	Station Name	Latitude	Longitude	Years Used
AAA	ALMA-ATA	43.250	76.917	1964-2002
AAE	ADDIS ABABA	9.033	38.767	1998-2003
ABG	ALIBAG	18.617	72.867	1889-2002
ABK	ABISKO	68.367	18.817	1966-2003
AIA	ARGENTINE ISLANDS (FARADAY)	-65.250	295.733	1959-2000
ALE	ALERT	82.500	297.650	1963-2001
AMS	AMSTERDAM ISLAND (MARTIN DE VIVIES)	-37.833	77.567	1983-2002
AMT	AMATSIA	31.550	34.917	1977-2000
API	APIA	-13.800	188.233	1912-2003
AQU	L'AQUILA	42.383	13.317	1961-2002
ARC	ARCTOWSKI	-62.167	301.517	1980-1995
ARS	ARTI	56.433	58.567	1891-2003
ASC	ASCENSION ISLAND	-7.950	345.617	1994-2000
ASH	ASHKHABAD (VANNOVSKAYA)	37.950	58.100	1960-2003
ASP	ALICE SPRINGS	-23.767	133.883	1994-2003
BDV	BUDKOV	49.067	14.017	1968-2003
BEL	BELSK	51.833	20.800	1961-2003
BFE	BRORFELDE	55.633	11.667	1908-2003
BJI	PEKING (BEIJING)	40.033	116.183	1958-1999
BJN	BEAR ISLAND (BJORNOYA)	74.500	19.000	1952-2002
BLC	BAKER LAKE	64.317	263.983	1953-2002
BMT	BEIJING MING TOMBS	40.300	116.200	1992-2002
BNG	BANGUI	4.433	18.567	1956-2002
BOU	BOULDER	40.133	254.767	1965-2003
BOX	BOROK	58.033	38.967	1978-2001
BRW	POINT BARROW	71.317	203.367	1964-2003
BSL	BAY ST LOUIS (STENNIS)	30.350	270.367	1988-2003
CBB	CAMBRIDGE BAY	69.117	254.967	1973-2002
CBI	CHICHIJIMA	27.100	142.183	1974-2002
CCS	CAPE CHELYUSKIN	77.717	104.283	1955-2000
CDP	CHENGDU	31.000	103.700	1983-2001
CLF	CHAMBON-LA-FORET	48.017	2.267	1901-2003
CMO	COLLEGE	64.867	212.133	1943-2003
CNB	CANBERRA	-35.317	149.367	1916-2003
CNH	CHANGCHUN (HELONG)	44.050	125.200	1958-1999
COI	COIMBRA (ALTO DA BALEIA)	40.217	351.583	1952-2003
CRP	CHIRIPA (TILARAN, COSTA RICA)	10.433	275.083	1986-1997
CTA	CHARTERS TOWERS	-20.083	146.267	1985-2003
CTS	CASTELLO TESINO	46.050	11.650	1966-1995
CWE	UELEN (CAPE WELLEN)	66.167	190.167	1955-1996
CZT	PORT ALFRED (CROZET)	-46.433	51.867	1975-2002

DIK	DIKSON ISLAND	73.550	80.567	1934-2000
DLN	DALIAN	39.100	121.500	1999-2001
DLR	DEL RIO	29.483	259.083	1984-2003
DOB	DOMBAS	62.067	9.117	1953-2002
DOU	DOURBES	50.100	4.600	1956-2003
DRV	DUMONT D'URVILLE	-66.667	140.017	1967-2002
EBR	EBRO (TORTOSA)	40.817	0.500	1996-2003
ELT	EILAT	29.667	34.950	1999-2001
ESA	ESASHI	39.233	141.350	1994-2002
ESK	ESKDALEMUIR	55.317	356.800	1934-2003
ETT	ETAIYAPURAM	9.167	78.017	1981-1998
EYR	EYREWELL	-43.417	172.350	1903-2003
FCC	FORT CHURCHILL	58.767	265.917	1965-2002
FRD	FREDERICKSBURG	38.200	282.617	1916-2003
FRN	FRESNO	37.083	240.283	1984-2003
FUQ	FUQUENE	5.467	286.267	1955-2000
FUR	FURSTENFELDBRUCK	48.167	11.283	1940-2003
GCK	GROCKA	44.633	20.767	1959-2000
GDH	GODHAVN	69.250	306.467	1927-2003
GLM	GOLMUD	36.400	94.900	1995-2000
GLN	GLENLEA	49.650	262.883	1983-1996
GNA	GNANGARA	-31.783	115.950	1920-2002
GUA	GUAM	13.583	144.867	1958-2003
GUI	GUIMAR (TENERIFE)	28.317	343.567	1960-2002
GZH	GUANGZHOU	23.100	113.350	1959-1997
HAD	HARTLAND	51.000	355.517	1935-2003
HBK	HARTEBEESTHOEK	-25.883	27.700	1974-2003
HER	HERMANUS	-34.417	19.233	1934-2003
HLP	HEL	54.600	18.817	1954-2003
HON	HONOLULU	21.317	202.000	1903-2003
HRB	HURBANOVO (O GYALLA, STARA DALA)	47.867	18.183	1942-2003
HRN	HORNSUND	77.000	15.550	1980-2003
HTY	HATIZYO (HACHIJOJIMA)	33.067	139.833	1981-2003
HUA	HUANCAYO	-12.050	284.683	2002-2003
HVN	LA HABANA (INST.GEOFIS.Y ASTRON.)	22.983	277.683	1999-1999
HYB	HYDERABAD	17.417	78.550	1965-1998
IQA	IQALUIT	63.750	291.483	1996-2002
IRK	PATRONY (IRKUTSK)	52.167	104.450	1888-2002
ISK	KANDILLI (ISTANBUL)	41.067	29.067	1949-1997
KAK	KAKIOKA	36.233	140.183	1940-2003
KDU	KAKADU	-12.683	132.467	1996-2003
KIR	KIRUNA	67.800	20.400	1971-1999
KIV	DYMER	50.717	30.300	1959-1998
KNY	KANOYA	31.417	130.883	1959-2003
KNZ	KANOZAN	35.250	139.967	1962-2002
KOD	KODAIKANAL	10.233	77.467	1952-1997

KOU	KOUROU	2.217	307.267	1997-2003
KRC	KARACHI	24.950	67.133	1986-2003
KSH	KASHI	39.500	76.000	1988-2000
LAS	LAS ACACIAS	-35.000	302.300	1963-1996
LER	LERWICK	60.133	358.817	1935-2003
LIV	LIVINGSTON ISLAND	-62.667	299.600	1997-2003
LMM	MAPUTO (LOURENCO MARQUES)	-25.917	32.583	1996-1999
LNN	VOEIKOVO (LENINGRAD)	59.950	30.700	1950-2000
LNP	LUNPING	25.000	121.167	1967-2000
LOV	LOVO	59.350	17.833	1929-2003
LRM	LEARMONTH	-22.217	114.100	1988-1998
LRV	LEIRVOGUR	64.183	338.300	1959-2003
LSA	LHASA	29.633	91.033	1984-1999
LVV	LVOV	49.900	23.750	1953-2001
LZH	LANZHOU	36.083	103.850	1965-2003
MAB	MANHAY	50.300	5.683	1984-2003
MAW	MAWSON	-67.600	62.883	1957-2001
MBC	MOULD BAY	76.317	240.633	1964-1996
MBO	M'BOUR	14.400	343.050	1954-2002
MCQ	MACQUARIE ISLAND	-54.500	158.950	1951-2003
MEA	MEANOOK	54.617	246.650	1960-2002
MGD	STEKOLNYY (MAGADAN)	60.117	151.017	1942-1998
MID	MIDWAY	28.200	182.617	2001-2001
MIR	MIRNY	-66.550	93.017	1961-2002
MIZ	MIZUSAWA	39.117	141.200	1973-2002
MMB	MEMAMBETSU	43.917	144.183	1953-2003
MNK	PLESHCHENITSI (MINSK)	54.500	27.883	1962-2000
MOL	MOLODYOZHNYAYA	-67.667	45.850	1967-1998
MOS	KRASNAYA PAKHRA (MOSCOW)	55.467	37.317	1947-2003
MZL	MANZHOU LI	49.600	117.400	1985-2001
NAL	NEW ALESUND	78.917	11.933	1967-2002
NAQ	NARSARSUAQ	61.167	314.567	1968-2003
NCK	NAGYCENK	47.633	16.717	1962-2003
NEW	NEWPORT	48.267	242.867	1968-2003
NGK	NIEMEGK	52.067	12.683	1894-2002
NGR	NAGPUR	21.150	79.083	1996-1998
NUR	NURMIJARVI	60.517	24.650	1954-2003
NVS	KLYUCHI (NOVOSIBIRSK)	55.033	82.900	1968-2003
ODE	ODESSA (STEPANOVKA)	46.783	30.883	1949-2000
ORC	ORCADAS DEL SUR (LAURIE ISLAND)	-60.733	315.217	2000-2001
OTT	OTTAWA	45.400	284.450	1970-2002
OUL	OULUJARVI	64.517	27.233	1994-2003
PAF	PORT-AUX-FRANCAIS (KERGUELEN)	-49.350	70.250	1958-2002
PAG	PANAGYURISHTTE	42.517	24.183	1949-2002
PBQ	POSTE-DE-LA-BALEINE	55.283	282.250	1967-2002
PET	PARATUNKA	53.100	158.633	1970-2002

PHU	PHUTHUY	21.033	105.950	1985-2003
PIL	PILAR	-31.667	296.117	1906-2001
PND	PONDICHERRY	11.917	79.917	1959-2001
PPT	PAMATAI (PAPEETE)	-17.567	210.417	1969-2002
PST	PORT STANLEY (FALKLAND ISLANDS)	-51.700	302.117	1995-2000
QGZ	QIONGZHONG	19.000	109.800	1983-1999
QIX	QIANLING	34.600	108.200	1985-2001
QSB	QSAYBEH	33.867	35.650	2001-2003
QUE	QUETTA	30.200	66.950	1955-2001
QZH	QUANZHOU	24.900	118.600	1983-1998
RES	RESOLUTE BAY	74.683	265.100	1960-2002
SAB	SABHAWALA	30.367	77.800	1965-2002
SBA	SCOTT BASE	-77.850	166.783	1960-2003
SFS	SAN FERNANDO	36.500	353.883	1992-2002
SHL	SHILLONG	25.567	91.883	1977-1995
SIT2	SITKA	57.050	224.667	1903-2003
SJG	SAN JUAN (PUERTO RICO)	18.100	293.850	1905-2003
SOD	SODANKYLA	67.367	26.633	1931-2003
SPT	SAN PABLO DE LOS MONTES	39.550	355.650	1948-2002
SSH	ZO-SE (SHESHAN)	31.100	121.183	1954-2000
STJ	ST. JOHNS	47.600	307.317	1970-2002
SUA	SURLARI	44.683	26.250	1951-2001
SYO	SYOWA STATION	-69.000	39.583	1959-2003
TAM	TAMANRASSET	22.800	5.533	1942-2003
TAN	TANANARIVE (ANTANANARIVO)	-18.917	47.550	1984-2002
TEO	TEOLOYUCAN	19.750	260.817	1924-1999
TFS	DUSHETI (TBILISI)	42.083	44.700	1939-2002
THJ	TONGHAI	24.000	102.700	1986-2001
THL	THULE (QANAQ)	77.467	290.767	1957-2003
THY	TIHANY	46.900	17.900	1950-2002
TIK	TIKSI	71.583	129.000	1945-1999
TKT	YANGI-BAZAR	41.333	69.617	1938-2003
TNB	TERRA NOVA BAY	-74.683	164.117	1987-1999
TNG	TANGERANG	-6.167	106.633	1951-1998
TRD	TRIVANDRUM	8.483	76.967	1959-1998
TRO	TROMSO	69.667	18.933	1931-2002
TRW	TRELEW	-43.267	294.617	1959-2003
TSU	TSUMEB	-19.200	17.583	1966-2002
TTB	TATUOCA	-1.200	311.483	1958-2003
TUC	TUCSON	32.167	249.267	1911-2003
UJJ	UJJAIN	23.183	75.783	1977-1998
VAL	VALENTIA	51.933	349.750	1900-2003
VIC	VICTORIA	48.517	236.583	1957-2002
VLA	GORNOTAYOZHNYAYA (VLADIVOSTOK)	43.683	132.167	1953-1997
VNA	NEUMAYER STATION	-70.667	351.733	1995-2002
VOS	VOSTOK	-78.450	106.867	1998-2002

VSK	VISAKHAPATNAM	17.667	83.317	1996-1998
VSS	VASSOURAS	-22.400	316.350	1932-2000
WHN	WUHAN	30.533	114.567	1960-2000
WIK	WIEN KOBENZL	48.267	16.317	1956-2001
WMQ	URUMQI (WULUMUCHI)	43.817	87.700	1979-2000
WNG	WINGST	53.750	9.067	1949-2003
YAK	YAKUTSK	62.017	129.717	1949-1997
YKC	YELLOWKNIFE	62.483	245.517	1976-2002

## 4. Modeling methods

A parent model is first fitted to all available data and can be used to synthesize magnetic field values for the duration of the data (1999.0-2004.5). Sections 4.1-4.5 describe its parameterization, its derivation, any necessary coordinate transformations, the prediction of secular variation and the weighting schemes used. Finally, Section 4.6 describes how the WMM2005 coefficients are derived.

### 4.1. Model parameterization

The geomagnetic field measured at the Earth's surface or at satellite altitude is the sum of the fields generated by sources internal or external to the solid Earth. Away from its sources, the internal magnetic field  $\mathbf{B}$  is a potential field and therefore can be written as the negative gradient of a scalar potential

$$\mathbf{B}(\varphi', \lambda, r, t) = -\nabla V(\varphi', \lambda, r, t). \quad (3)$$

This potential can be expanded in terms of spherical harmonics:

$$V(\varphi', \lambda, r, t) = a \left\{ \sum_{n=1}^N \sum_{m=0}^n (g_n^m(t) \cos(m\lambda) + h_n^m(t) \sin(m\lambda)) \left( \frac{a}{r} \right)^{n+1} \check{P}_n^m(\sin \varphi') \right\} \quad (4)$$

where  $a$  (6371.2 km) is the standard Earth's magnetic reference radius,  $(\varphi', \lambda, r)$  are the latitude, longitude and radius in a spherical, geocentric reference frame, and  $(g_n^m(t), h_n^m(t))$  are the time-dependent Gauss coefficients of degree  $n$  and order  $m$  describing internal sources.

$P_n^m(\sin \varphi')$  are the Schmidt semi-normalized Associated Legendre Functions (Gradsteyn and Ryzhik, 1994), defined as

$$\begin{aligned} \tilde{P}_n^m(\sin \varphi') &= \sqrt{2 \frac{(n-m)!}{(n+m)!}} P_n^m(\sin \varphi') \quad \text{if } m > 0 \\ \tilde{P}_n^m(\sin \varphi') &= P_n^m(\sin \varphi') \quad \text{if } m = 0 \end{aligned} \quad (5)$$

We used  $N = 36$  as the truncation level of the internal expansion. The internal Gauss coefficients from degree 1 to 8 are assumed to have a quadratic dependence on time,

$$\begin{aligned} g_n^m(t) &= g_n^m + \dot{g}_n^m(t-t_0) + \frac{1}{2} \ddot{g}_n^m(t-t_0)^2 \\ h_n^m(t) &= h_n^m + \dot{h}_n^m(t-t_0) + \frac{1}{2} \ddot{h}_n^m(t-t_0)^2 \end{aligned} \quad (6)$$

where, on the left side,  $g_n^m(t)$  and  $h_n^m(t)$  are time varying functions, while  $g_n^m$ ,  $h_n^m$ ,  $\dot{g}_n^m$ ,  $\dot{h}_n^m$ ,  $\ddot{g}_n^m$ , and  $\ddot{h}_n^m$  on the right side of equation (6) denote constants. The time is given in decimal year and  $t_0$  is the reference date of the model, chosen to be at the approximate mid-point of the time span of satellite and observatory hourly mean values (2002.0). From degree 9 up to 12 a linear dependence on time of the internal Gauss coefficients is assumed, and, for higher degrees, the internal Gauss coefficients are assumed to be constant with time. These truncation levels are chosen as the degrees up to which coefficients can be determined robustly without recourse to damping.

This model given by equation (4) is valid only for sources internal to the Earth, like the main field and the crustal field. For the external field, caused by currents in the ionosphere and magnetosphere, a spherical harmonic representation similar to equation (4) can be used. However, the external fields are organized in a sun synchronous reference frame. Our parent model includes a constant degree-2 parameterization of magnetospheric fields in a sun-synchronous reference frame. For an earth-fixed, rotating observer, these external fields are perceived to have daily and seasonal variations. Our parent model accounts for these periodic variations, as well as for their electromagnetic induction in the Earth. For further details, see Sabaka et al. (2002), Lesur et al. (2004) and forthcoming publications.

A Dst dependence for the degree 1 external Gauss coefficients is introduced to represent the variability of the magnetospheric ring current. This current system induces an internal magnetic field that can be partially modeled by time-varying degree 1 internal Gauss coefficients. The internal/external Dst separation was done using the procedure of Maus and Weidelt (2004), based on the semi-global Earth conductivity model of Utada et al. (2003).

Following evidence of a penetration of the Interplanetary Magnetic Field (IMF), as shown in Lesur et al. (2004), an IMF  $B_y$  correlated component in a sun-synchronous reference frame was included in the modeling. This component reaches about half of the IMF  $B_y$  at the Earth's surface, with typical strengths of 1-2 nT.

Tidal movement of conducting seawater through the Earth's magnetic field induces electric fields, currents, and secondary magnetic fields, which reach about 7 nT at the ocean surface and 3 nT at satellite altitude. These fields are clearly visible in satellite data and closely coincide with independent predictions from tidal ocean flow models (Tyler et al., 2003). The satellite measurements were corrected for the eight major tidal constituents, using the modeling method of Maus and Kuvshinov (2004).

Finally, when the data set contains hourly mean observatory data, offsets at each observatory have to be introduced to take into account the local field, mainly generated in the crust, which cannot be described by the model. Then, at an observatory, the magnetic field  $\mathbf{B}$  is:

$$\mathbf{B}(\varphi', \lambda, r, t) = -\nabla V(\varphi', \lambda, r, t) + \mathbf{O}(\varphi', \lambda, r) \quad (7)$$

where the offset vector  $\mathbf{O}(\varphi', \lambda, r)$ , also referred to as crustal bias, is constant in time.

The above parameterization is used to fit data sets selected from satellite measurements and observatory hourly mean values. The equations for the internal part of the field are:

$$X'(\varphi', \lambda, r) = -\frac{1}{r} \frac{\partial V}{\partial \varphi'} = -\sum_{n=1}^N \left(\frac{a}{r}\right)^{n+2} \sum_{m=0}^n (g_n^m(t) \cos m\lambda + h_n^m(t) \sin m\lambda) \frac{d\check{P}_n^m(\sin \varphi')}{d\varphi'} \quad (8)$$

$$Y'(\varphi', \lambda, r) = -\frac{1}{r \cos \varphi'} \frac{\partial V}{\partial \lambda} = \frac{1}{\cos \varphi'} \sum_{n=1}^N \left(\frac{a}{r}\right)^{n+2} \sum_{m=0}^n m (g_n^m(t) \sin m\lambda - h_n^m(t) \cos m\lambda) \check{P}_n^m(\sin \varphi') \quad (9)$$

$$Z'(\varphi', \lambda, r) = \frac{\partial V}{\partial r} = -\sum_{n=1}^N (n+1) \left(\frac{a}{r}\right)^{n+2} \sum_{m=0}^n (g_n^m(t) \cos m\lambda + h_n^m(t) \sin m\lambda) \check{P}_n^m(\sin \varphi') \quad (10)$$

## 4.2. Model determination

The above equations, with the magnetic field vector observations on the left-hand side, form the equations of condition. Thus, if there are  $D$  data, there are  $D$  linear equations with the  $P$  parameters of the parent model:

$$\mathbf{y} = \mathbf{A}\mathbf{m} \quad (11)$$

where  $\mathbf{y}$  is the column vector ( $D \times 1$ ) of observations,  $\mathbf{A}$  is the matrix ( $D \times P$ ) of coefficients to the unknowns which are functions of position, and  $\mathbf{m}$  is the column vector ( $P \times 1$ ) of unknowns, the Gauss coefficients of the model. As there are many more observations than unknowns, i.e. as  $D > P$ , the system is over-determined and therefore does not have an exact solution. Suppose  $\tilde{\mathbf{m}}$  is an estimate of  $\mathbf{m}$ . Then

$$\tilde{\mathbf{y}} = \mathbf{A}\tilde{\mathbf{m}} \quad (12)$$

where  $\tilde{\mathbf{y}}$  are estimates of the observations. The residuals are  $\mathbf{y} - \tilde{\mathbf{y}}$  and the least-squares method requires that  $\tilde{\mathbf{m}}$  is chosen so as to minimize the weighted sum of the squares of the residuals,  $S$ , i.e.:

$$\begin{aligned} \text{minimize } S &= (\mathbf{y} - \tilde{\mathbf{y}})^T \mathbf{W}(\mathbf{y} - \tilde{\mathbf{y}}) \\ &= (\mathbf{y} - \mathbf{A}\tilde{\mathbf{m}})^T \mathbf{W}(\mathbf{y} - \mathbf{A}\tilde{\mathbf{m}}) \quad \text{with respect to } \tilde{\mathbf{m}}. \end{aligned}$$

$\mathbf{W}$  is the weight matrix ( $D \times D$ ) of the data. For Ørsted data there are off-diagonal terms in this matrix to account for the anisotropic errors arising from the star camera (Holme, 2000). The

minimum is reached when  $\frac{\partial S}{\partial \tilde{\mathbf{m}}} = 0$ . Now

$$\begin{aligned}
\frac{\partial S}{\partial \tilde{\mathbf{m}}} &= \lim_{\delta \tilde{\mathbf{m}} \rightarrow \mathbf{0}} \frac{S(\tilde{\mathbf{m}} + \delta \tilde{\mathbf{m}}) - S(\tilde{\mathbf{m}})}{\delta \tilde{\mathbf{m}}} \\
&= \lim_{\delta \tilde{\mathbf{m}} \rightarrow \mathbf{0}} \frac{(\mathbf{y} - \mathbf{A}(\tilde{\mathbf{m}} + \delta \tilde{\mathbf{m}}))^T \mathbf{W}(\mathbf{y} - \mathbf{A}(\tilde{\mathbf{m}} + \delta \tilde{\mathbf{m}})) - (\mathbf{y} - \mathbf{A}\tilde{\mathbf{m}})^T \mathbf{W}(\mathbf{y} - \mathbf{A}\tilde{\mathbf{m}})}{\delta \tilde{\mathbf{m}}} \\
&= \lim_{\delta \tilde{\mathbf{m}} \rightarrow \mathbf{0}} \frac{(\mathbf{z} - \mathbf{A}\delta \tilde{\mathbf{m}})^T \mathbf{W}(\mathbf{z} - \mathbf{A}\delta \tilde{\mathbf{m}}) - \mathbf{z}^T \mathbf{W}\mathbf{z}}{\delta \tilde{\mathbf{m}}} \quad \text{where } \mathbf{z} = \mathbf{y} - \mathbf{A}\tilde{\mathbf{m}} \\
&= \lim_{\delta \tilde{\mathbf{m}} \rightarrow \mathbf{0}} \frac{-2\delta \tilde{\mathbf{m}}^T \mathbf{A}^T \mathbf{W}\mathbf{z} + O(\delta \tilde{\mathbf{m}}^2)}{\delta \tilde{\mathbf{m}}} \\
&= 0 \quad \text{when } \mathbf{A}^T \mathbf{W}\mathbf{z} = \mathbf{0}
\end{aligned}$$

i.e. when  $\mathbf{A}^T \mathbf{W}\mathbf{A}\tilde{\mathbf{m}} = \mathbf{A}^T \mathbf{W}\mathbf{y}$ .

These are the normal equations and the estimated unknowns  $\tilde{\mathbf{m}}$  are found from

$$\tilde{\mathbf{m}} = (\mathbf{A}^T \mathbf{W}\mathbf{A})^{-1} \mathbf{A}^T \mathbf{W}\mathbf{y}. \quad (13)$$

As there are total intensity observations included in the dataset and these data are not linear functions of the unknowns, one has to linearize the problem and the process becomes iterative. The iteration is continued till the differences between the estimated unknowns  $\tilde{\mathbf{m}}$  are negligible.

### 4.3. Coordinate transformation

Satellite data are already located in a geocentric coordinate system but surface data are almost invariably located in a geodetic coordinate system, i.e. relative to the mean sea surface of the Earth, which can be approximated by an ellipsoid. The locations of surface data, and the data themselves, must be transformed from geodetic to geocentric coordinates prior to spherical harmonic modeling.

When computing the model, the locations  $(h, \varphi, \lambda)$ , where  $h$  is the geodetic altitude and  $\varphi$  is the geodetic latitude, are transformed into  $(r, \varphi', \lambda)$  using

$$\tan \varphi' = \frac{(A^2 \cos^2 \varphi + B^2 \sin^2 \varphi)^{1/2} h + B^2}{(A^2 \cos^2 \varphi + B^2 \sin^2 \varphi)^{1/2} h + A^2} \tan \varphi \quad (14)$$

$$r^2 = h^2 + 2h(A^2 \cos^2 \varphi + B^2 \sin^2 \varphi)^{1/2} + \frac{A^4 \cos^2 \varphi + B^4 \sin^2 \varphi}{A^2 \cos^2 \varphi + B^2 \sin^2 \varphi} \quad (15)$$

where  $A=6378.137$  km is the semi-major axis (equatorial radius) of the ellipsoid and  $B=6356.7523142$  km is the semi-minor axis as defined by the World Geodetic System 1984 (WGS84).

The observations of the northerly, easterly and vertically down intensities  $X, Y,$  and  $Z,$  relative to an ellipsoid, are transformed into the northerly, easterly and vertically down intensities relative to a sphere,  $X', Y',$  and  $Z'$ :

$$\begin{aligned} X' &= X \cos \psi + Z \sin \psi \\ Y' &= Y \\ Z' &= -X \sin \psi + Z \cos \psi \end{aligned} \quad (16)$$

where  $\psi$  is the difference between geocentric and geodetic latitude in the sense  $\psi = \varphi' - \varphi$ .

Another coordinate system used in global magnetic field modeling is the geomagnetic coordinate system. This is used in the derivation of WMM2005 to identify data locations within a certain latitude band of the geomagnetic equator for which vector data values are required. This coordinate system is based on the internal centered dipolar field and is defined by the first three main-field coefficients of an existing global spherical harmonic model. Its reference axis is aligned along the dipole axis, which is tilted from the rotational axis of the Earth by about  $11^\circ$  and cuts the surface of the Earth at the geomagnetic poles. The geomagnetic equator is the

great circle  $90^\circ$  from the geomagnetic poles and geomagnetic latitude varies from  $0^\circ$  at the geomagnetic equator to  $\pm 90^\circ$  at the geomagnetic poles.

#### **4.4. Secular variation prediction**

Predictions of future changes in the magnetic field were derived from the long-term observatory annual mean data as well as polynomial extrapolation of the parent model based on satellite data and observatory hourly mean values. Annual mean data were utilised by determining and applying linear predictor filters to series of first differences to result in estimates of secular variation up to 2010.0 (Macmillan and Quinn, 2000). Linear prediction is successful at extrapolating signals which are smooth and oscillatory, though not necessarily periodic, and tests have shown that when predicting more than about 3 years ahead, this method is better than linear regression applied to recent first differences (equivalent to quadratic polynomial fitted to annual means). For incorporation into the final secular-variation model we used averages of the predictions for 2005.0-2010.0 at 159 observatories with sufficiently long time series. They were assigned uncertainties that reflected the past success of prediction for the data series in question. Data from 29 observatories, which had time series too short for the application of linear prediction filters, were also used by computing average secular-variation estimates and assuming that these did not change with time.

#### **4.5. Data weighting schemes**

One of the major difficulties when building a geomagnetic field model is to estimate the weights to be given to each of the different data sets and, within the data sets themselves, the weights for each data value. In principle, the data should be weighted by the inverse of the measurement error variance but usually these variances are unknown. Furthermore, geomagnetic field models do not model all sources of the measured magnetic field so the data weights must take into account these unmodeled signals. Again, estimating accurately the amplitude of these signals is very difficult, if not impossible. To account for the higher data density close to the poles and the increase in the noise level in high latitudes, the satellite data are down-weighted in these regions. A similar approach is used for observatory data whose distribution is dense in Western Europe and North America and sparser in the Southern Hemisphere.

The high latitude ionosphere experiences a continuous precipitation of charged particles, causing a high conductivity, even during complete darkness. Distant magnetospheric electric fields are mapped down into the polar ionosphere, driving various current systems. These systems of currents are highly variable but are always present even for magnetically quiet periods. Therefore data acquired in these areas have to be down-weighted according to the presumed noise level. Similarly, data acquired at dawn and dusk are noisier than those acquired in the middle of the night, especially at high latitudes, and the weights are adjusted to take that into account. A high density of satellite data at high latitudes and gaps at the poles arise from the satellite orbit characteristics. Further irregularities in spatial data coverage arise from the selection of quiet time data. To compensate for unequal spatial data coverage, datum numbers were counted for equal area bins and the data in each bin were downweighted by the count in order to maintain equal area weighting. Uniform spatial weighting on the sphere improves the separation of internal and external fields in the least squares estimation. We also account for the anisotropy in the attitude accuracy of Ørsted vector data, as detailed in Holme (2000).

For the secular-variation models, two different synthetic data sets were used and in these data sets, the data were weighted by the inverse of the square of the estimated error. For the data derived from the long time series of observatory secular variation, error assignments were based on actual past prediction errors (up to a maximum lead time of 10 years), both globally and locally. For the synthetic data derived from satellite and observatory hourly mean data sets, the errors were estimated from the formal standard deviations of the underlying model Gauss coefficients, and were then increased because they are known to be too small (Loves and Olsen, 2004). However, these data were on average given higher weights in the final model than the predicted observatory secular variation values.

#### **4.6. Derivation of WMM2005**

The final main-field coefficients for 2005.0 were derived by polynomial extrapolation of the main-field Gauss coefficients from the parent model to this date, using equation (6).

Before the final secular-variation coefficients could be derived, the secular-variation estimates from the parent model (valid for 1999.0-2004.5) were combined with the long-term predictions at the observatories described in Section 4.4. This was done by using the parent model to estimate annual rates of change in the north, east and vertically down directions, in a geocentric coordinate system, at the centers of 1654 equal-area tesserae. Each tessera was equivalent in size to a 5° latitude by 5° longitude box at the equator. This synthetic dataset was combined with the predicted mean  $X$ ,  $Y$  and  $Z$  rates of change for 2005.0-2010.0 at the 188 observatories, rotated into a geocentric coordinate system. Equations (8)-(10) of Section 4.1, with the time-varying Gauss coefficients  $g_n^m(t)$ ,  $h_n^m(t)$  replaced by their time derivatives  $\dot{g}_n^m$  and  $\dot{h}_n^m$ , were then used to determine the final secular-variation coefficients, using the weighting scheme as described in Section 4.4. The final coefficients are listed in Table 4 of Section 5.1.

## 5. Resulting model

This section lists the final model coefficients, the corresponding magnetic pole and eccentric dipole locations, provides the equations for computing the magnetic field components at a given location, and discusses the accuracy and limitations of the model.

At the end of this report, a series of contour maps is presented for all of the geomagnetic elements and their annual rates of change. Maps are presented in Mercator projection of the world between +/- 70° latitude, and in Polar Stereographic projection. These charts are also available in digital format on the CD-ROM and the WMM Web site at:

<http://www.ngdc.noaa.gov/seg/WMM/>.

### 5.1. Model coefficients

The model coefficients, also referred to as Gauss coefficients, provide an accurate and convenient representation of the Earth's main magnetic field. Their values are listed in Table 4. These coefficients can be used to compute values for the field elements and their annual rates of change at any location near the surface of the Earth and at any date between 2005.0 and 2010.0. A step-by-step guide to the magnetic field computation is given in Section 5.3.

**Table 4: Final coefficients for WMM2005 Units are nT for the main field at 2005.0, and nT per year for the secular variation (SV) 2005.0-2010.0. Coefficients  $g$  and  $h$  are arranged by increasing degree,  $n$ , and order,  $m$ .**

$n$	$m$	$g_n^m$	$h_n^m$	$\dot{g}_n^m$	$\dot{h}_n^m$
1	0	-29556.8		8.0	
1	1	-1671.7	5079.8	10.6	-20.9
2	0	-2340.6		-15.1	
2	1	3046.9	-2594.7	-7.8	-23.2
2	2	1657.0	-516.7	-0.8	-14.6
3	0	1335.4		0.4	
3	1	-2305.1	-199.9	-2.6	5.0
3	2	1246.7	269.3	-1.2	-7.0
3	3	674.0	-524.2	-6.5	-0.6
4	0	919.8		-2.5	
4	1	798.1	281.5	2.8	2.2
4	2	211.3	-226.0	-7.0	1.6
4	3	-379.4	145.8	6.2	5.8
4	4	100.0	-304.7	-3.8	0.1
5	0	-227.4		-2.8	
5	1	354.6	42.4	0.7	0.0
5	2	208.7	179.8	-3.2	1.7
5	3	-136.5	-123.0	-1.1	2.1
5	4	-168.3	-19.5	0.1	4.8
5	5	-14.1	103.6	-0.8	-1.1
6	0	73.2		-0.7	
6	1	69.7	-20.3	0.4	-0.6
6	2	76.7	54.7	-0.3	-1.9
6	3	-151.2	63.6	2.3	-0.4
6	4	-14.9	-63.4	-2.1	-0.5
6	5	14.6	-0.1	-0.6	-0.3
6	6	-86.3	50.4	1.4	0.7
7	0	80.1		0.2	
7	1	-74.5	-61.5	-0.1	0.6
7	2	-1.4	-22.4	-0.3	0.4
7	3	38.5	7.2	1.1	0.2
7	4	12.4	25.4	0.6	0.3
7	5	9.5	11.0	0.5	-0.8
7	6	5.7	-26.4	-0.4	-0.2
7	7	1.8	-5.1	0.6	0.1
8	0	24.9		0.1	
8	1	7.7	11.2	0.3	-0.2
8	2	-11.6	-21.0	-0.4	0.1
8	3	-6.9	9.6	0.3	0.3
8	4	-18.2	-19.8	-0.3	0.4

8	5	10.0	16.1	0.2	0.1
8	6	9.2	7.7	0.4	-0.2
8	7	-11.6	-12.9	-0.7	0.4
8	8	-5.2	-0.2	0.4	0.4
9	0	5.6		0.0	
9	1	9.9	-20.1	0.0	0.0
9	2	3.5	12.9	0.0	0.0
9	3	-7.0	12.6	0.0	0.0
9	4	5.1	-6.7	0.0	0.0
9	5	-10.8	-8.1	0.0	0.0
9	6	-1.3	8.0	0.0	0.0
9	7	8.8	2.9	0.0	0.0
9	8	-6.7	-7.9	0.0	0.0
9	9	-9.1	6.0	0.0	0.0
10	0	-2.3		0.0	0.0
10	1	-6.3	2.4	0.0	0.0
10	2	1.6	0.2	0.0	0.0
10	3	-2.6	4.4	0.0	0.0
10	4	0.0	4.8	0.0	0.0
10	5	3.1	-6.5	0.0	0.0
10	6	0.4	-1.1	0.0	0.0
10	7	2.1	-3.4	0.0	0.0
10	8	3.9	-0.8	0.0	0.0
10	9	-0.1	-2.3	0.0	0.0
10	10	-2.3	-7.9	0.0	0.0
11	0	2.8		0.0	0.0
11	1	-1.6	0.3	0.0	0.0
11	2	-1.7	1.2	0.0	0.0
11	3	1.7	-0.8	0.0	0.0
11	4	-0.1	-2.5	0.0	0.0
11	5	0.1	0.9	0.0	0.0
11	6	-0.7	-0.6	0.0	0.0
11	7	0.7	-2.7	0.0	0.0
11	8	1.8	-0.9	0.0	0.0
11	9	0.0	-1.3	0.0	0.0
11	10	1.1	-2.0	0.0	0.0
11	11	4.1	-1.2	0.0	0.0
12	0	-2.4		0.0	0.0
12	1	-0.4	-0.4	0.0	0.0
12	2	0.2	0.3	0.0	0.0
12	3	0.8	2.4	0.0	0.0
12	4	-0.3	-2.6	0.0	0.0
12	5	1.1	0.6	0.0	0.0
12	6	-0.5	0.3	0.0	0.0
12	7	0.4	0.0	0.0	0.0

12	8	-0.3	0.0	0.0	0.0
12	9	-0.3	0.3	0.0	0.0
12	10	-0.1	-0.9	0.0	0.0
12	11	-0.3	-0.4	0.0	0.0
12	12	-0.1	0.8	0.0	0.0

## 5.2. Magnetic pole and eccentric dipole locations

The geomagnetic poles, otherwise known as the dipole poles, can be computed from the first three Gauss coefficients. From the WMM2005 coefficients for 2005.0 the geomagnetic north pole is at longitude 71.78°W and geodetic latitude 79.74°N and the geomagnetic south pole is at longitude 108.22°E and geodetic latitude 79.74°S.

The magnetic poles, otherwise known as the dip poles, are computed from all the Gauss coefficients using an iterative method. At 2005.0 the north magnetic pole is located at longitude 118.32°W and geodetic latitude 83.21°N and the south magnetic pole is at longitude 137.86°E and geodetic latitude 64.53°S. In practice the geomagnetic field is not exactly vertical at these dip poles but is vertical on oval-shaped loci traced on a daily basis, with considerable variation from one day to another, and approximately centered on the dip pole positions.

The location of the center of the eccentric dipole, sometimes known as the magnetic center, computed using the first eight Gauss coefficients for 2005.0, is at approximately  $(r, \varphi', \lambda) = (552 \text{ km}, 22.2^\circ\text{N}, 141.6^\circ\text{E})$ .

## 5.3. Equations for computing the magnetic field elements

A step by step procedure is given for computing the magnetic field elements at a given location and time  $(h, \varphi, \lambda, t)$ , where  $h$  is the geodetic altitude,  $\varphi$  and  $\lambda$  are the geodetic latitude and longitude, and  $t$  is the time given in decimal year.

In the first step, the ellipsoidal geodetic coordinates  $(h, \varphi, \lambda)$  are transformed into spherical geocentric coordinates  $(r, \varphi', \lambda)$  using

$$\tan \varphi' = \frac{(A^2 \cos^2 \varphi + B^2 \sin^2 \varphi)^{1/2} h + B^2}{(A^2 \cos^2 \varphi + B^2 \sin^2 \varphi)^{1/2} h + A^2} \tan \varphi \quad (17)$$

$$r^2 = h^2 + 2h(A^2 \cos^2 \varphi + B^2 \sin^2 \varphi)^{1/2} + \frac{A^4 \cos^2 \varphi + B^4 \sin^2 \varphi}{A^2 \cos^2 \varphi + B^2 \sin^2 \varphi} \quad (18)$$

where  $A=6378.137$  km is the semi-major axis (equatorial radius) of the ellipsoid and  $B=6356.7523142$  km is the semi-minor axis referenced to the WGS84 ellipsoid.

In the second step, the Gauss coefficients  $(g_n^m(t), h_n^m(t))$  of degree  $n$  and order  $m$  are determined for the desired time. This is achieved by adjusting the coefficients  $(g_n^m, h_n^m)$  of the field at  $t_0 = 2005.0$  for the linear secular variation  $(\dot{g}_n^m, \dot{h}_n^m)$ , as

$$\begin{aligned} g_n^m(t) &= g_n^m + \dot{g}_n^m(t - t_0) \\ h_n^m(t) &= h_n^m + \dot{h}_n^m(t - t_0) \end{aligned} \quad (19)$$

where the time is given in decimal year and  $t_0 = 2005.0$  is the reference date of the model.

In the third step, the field vector components  $X'$ ,  $Y'$  and  $Z'$  in geocentric coordinates are computed as

$$X'(\varphi', \lambda, r) = -\frac{1}{r} \frac{\partial V}{\partial \varphi'} = -\sum_{n=1}^{12} \left(\frac{a}{r}\right)^{n+2} \sum_{m=0}^n (g_n^m(t) \cos m\lambda + h_n^m(t) \sin m\lambda) \frac{d\check{P}_n^m(\sin \varphi')}{d\varphi'} \quad (20)$$

$$Y'(\varphi', \lambda, r) = -\frac{1}{r \cos \varphi'} \frac{\partial V}{\partial \lambda} = \frac{1}{\cos \varphi'} \sum_{n=1}^{12} \left(\frac{a}{r}\right)^{n+2} \sum_{m=0}^n m(g_n^m(t) \sin m\lambda - h_n^m(t) \cos m\lambda) \check{P}_n^m(\sin \varphi') \quad (21)$$

$$Z'(\varphi', \lambda, r) = \frac{\partial V}{\partial r} = -\sum_{n=1}^{12} (n+1) \left(\frac{a}{r}\right)^{n+2} \sum_{m=0}^n (g_n^m(t) \cos m\lambda + h_n^m(t) \sin m\lambda) \check{P}_n^m(\sin \varphi') \quad (22)$$

At this point, one can also compute the secular variation of the field components as

$$\dot{X}'(\varphi', \lambda, r) = -\frac{1}{r} \frac{\partial \dot{V}}{\partial \varphi'} = -\sum_{n=1}^{12} \left(\frac{a}{r}\right)^{n+2} \sum_{m=0}^n (\dot{g}_n^m \cos m\lambda + \dot{h}_n^m \sin m\lambda) \frac{d\check{P}_n^m(\sin \varphi')}{d\varphi'} \quad (23)$$

$$\dot{Y}'(\varphi', \lambda, r) = -\frac{1}{r \cos \varphi'} \frac{\partial \dot{V}}{\partial \lambda} = \frac{1}{\cos \varphi'} \sum_{n=1}^{12} \left(\frac{a}{r}\right)^{n+2} \sum_{m=0}^n m(\dot{g}_n^m \sin m\lambda - \dot{h}_n^m \cos m\lambda) \check{P}_n^m(\sin \varphi') \quad (24)$$

$$\dot{Z}'(\varphi', \lambda, r) = \frac{\partial \dot{V}}{\partial r} = -\sum_{n=1}^{12} (n+1) \left(\frac{a}{r}\right)^{n+2} \sum_{m=0}^n (\dot{g}_n^m \cos m\lambda + \dot{h}_n^m \sin m\lambda) \check{P}_n^m(\sin \varphi') \quad (25)$$

In the fourth step, the geocentric vector components  $X'$ ,  $Y'$  and  $Z'$  are transformed back into the geodetic reference frame, using

$$\begin{aligned} X &= X' \cos \psi - Z' \sin \psi \\ Y &= Y' \\ Z &= X' \sin \psi + Z' \cos \psi \end{aligned} \quad (26)$$

where  $\psi = \varphi' - \varphi$  is the difference between geocentric and geodetic latitude and  $\varphi'$  was computed in step 1. Similarly, the time derivatives of the vector components are transformed using

$$\begin{aligned} \dot{X} &= \dot{X}' \cos \psi - \dot{Z}' \sin \psi \\ \dot{Y} &= \dot{Y}' \\ \dot{Z} &= \dot{X}' \sin \psi + \dot{Z}' \cos \psi \end{aligned} \quad (27)$$

In the last step, the magnetic elements  $H$ ,  $F$ ,  $D$ ,  $I$ , and the grid variation,  $GV$ , are computed from the vector components as

$$\begin{aligned} H &= \sqrt{X^2 + Y^2}, \quad F = \sqrt{H^2 + Z^2}, \quad D = \arctan(Y, X), \quad I = \arctan(Z, H), \\ GV &= D - \lambda \quad \text{for } \varphi > 55^\circ, \quad GV = D + \lambda \quad \text{for } \varphi < -55^\circ \end{aligned} \quad (28)$$

where  $\arctan(a, b)$  is  $\tan^{-1}(a/b)$ , taking into account the angular quadrant, avoiding a division by zero, and resulting in a declination in the range of  $-180^\circ$  to  $180^\circ$  and inclination of  $-90^\circ$  to  $90^\circ$ . For  $H=0$  the declination is undefined.

The secular variation of these elements is computed using

$$\begin{aligned}
 \dot{H} &= \frac{X \cdot \dot{X} + Y \cdot \dot{Y}}{H} \\
 \dot{F} &= \frac{X \cdot \dot{X} + Y \cdot \dot{Y} + Z \cdot \dot{Z}}{F} \\
 \dot{D} &= \frac{180}{\pi} \frac{X \cdot \dot{Y} - Y \cdot \dot{X}}{H^2} \\
 \dot{i} &= \frac{180}{\pi} \frac{H \cdot \dot{Z} - Z \cdot \dot{H}}{F^2} \\
 G\dot{V} &= \dot{D}
 \end{aligned} \tag{29}$$

where  $\dot{D}$ ,  $\dot{i}$ , and  $G\dot{V}$  are given in degrees/year. Here, the factor  $\frac{180}{\pi}$  converts from radians to degree. This conversion factor is not present in equation (28), assuming that the arctan function provides the result in degrees.

#### 5.4. Model accuracy

First, we assessed the accuracy of the parent model, which includes parts of the external, induced and crustal fields, using a greater number of coefficients, and including crustal biases for the observatories. Statistics of the differences between the parent model and the input data are given in Table 5.

Next, we verified the accuracy and consistency of the estimated WMM coefficients by independently estimating the WMM coefficients from CHAMP and Ørsted satellite data and comparing the results. As shown in Figures 9 and 10, the resulting differences in  $D$  and in  $F$  are extremely small, indicating the high accuracy and consistency of the measurements of the two satellites.

**Table 5: Statistics of parent model residuals for different types of input data**

		<i>X</i>	<i>Y</i>	<i>Z</i>	<i>F</i>
Ørsted satellite	Number	37482	37482	37482	8920
	Residual mean (nT)	-0.1	0.4	-0.1	-1.0
	Residual rms (nT)	6.8	6.5	5.4	5.8
Champ satellite	Number	26754	26754	26754	5582
	Residual mean (nT)	1.0	0.1	-0.5	-3.4
	Residual rms (nT)	5.8	4.5	4.4	8.2
All satellites	Number	64236	64236	64236	14502
	Residual mean (nT)	0.4	0.3	-0.3	-1.9
	Residual rms (nT)	6.4	5.7	5.0	6.9
Observatories	Number	80874	80874	80874	39901
	Residual mean (nT)	0.0	0.0	0.0	0.7
	Residual rms (nT)	5.5	4.6	3.5	19.1

Finally, we compared the prediction of the old WMM2000 at the end of its life span in 2005.0 with the new WMM2005. Figure 11 shows the differences between WMM2005 and WMM2000 at 2005.0 for all magnetic elements. The global RMS difference for total intensity is less than 100 nT. This latter Figure demonstrates that WMM2000 *did* comply with the accuracy requirements (in terms of fitting the main field) over its lifetime rather than showing that WMM2005 *will* comply. However past performance is a good indicator of future performance and, while unforeseen changes in the dynamics of the field (e.g. jerks) are possible, the input satellite dataset for WMM2005 is far superior to that for WMM2000.

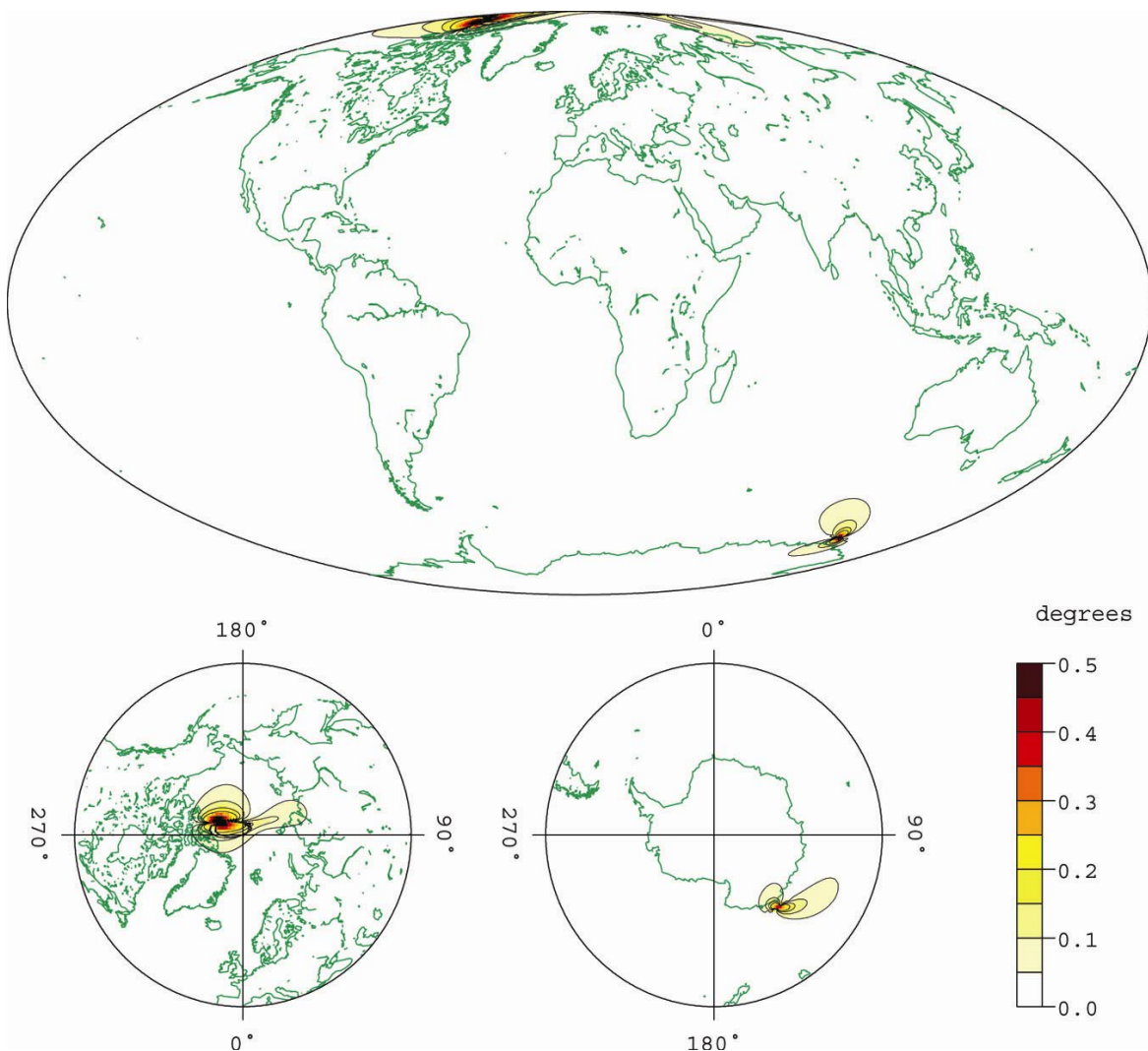


**Figure 9: Difference in declination between independent Ørsted and CHAMP models for 2005.0 at the Earth's surface. Contour interval 0.05°.**

Therefore, from a global perspective, the declination ( $D$ ), inclination ( $I$ ), and grid variation ( $GV$ ) RMS errors of WMM2005 are estimated to be less than 1.0° at the Earth's surface over the entire 5-year life span of the model. Also, the RMS errors at the Earth's surface horizontal intensity ( $H$ ), the vertical component ( $Z$ ), and the total intensity ( $F$ ) of WMM2005 are estimated to be well below 200 nT over the entire 5-year life of the model. Thus, the accuracy of the WMM2005 will meet and exceed the accuracy requirements detailed in MIL-W-89500 (Defense Mapping Agency, 1993) for the entire life span of the model.

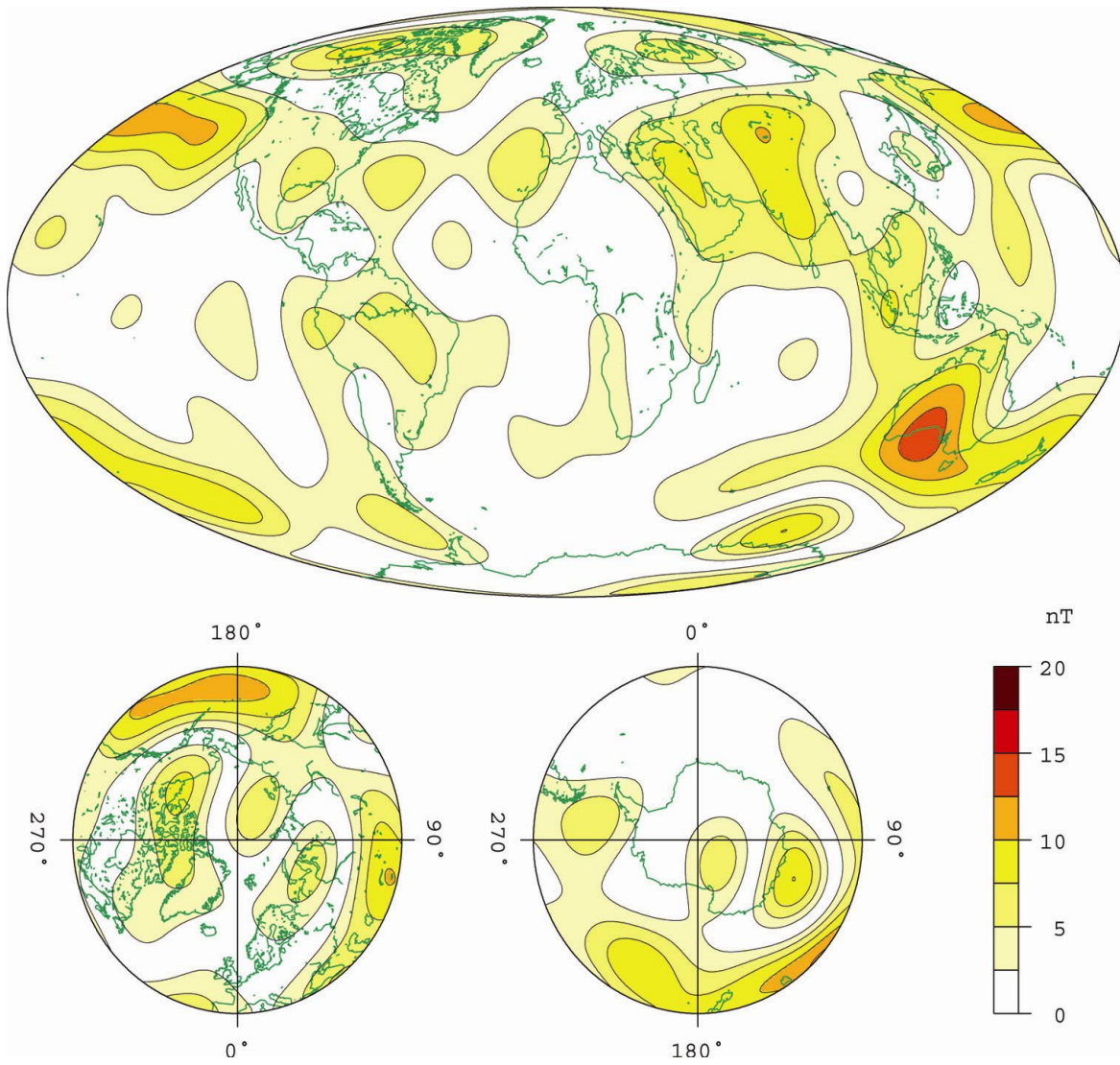


**Figure 10: Estimated error in the strength of the total intensity (F) for the WMM 2005.0, given by the difference between independent Ørsted and CHAMP models for 2005 at the Earth's surface.**

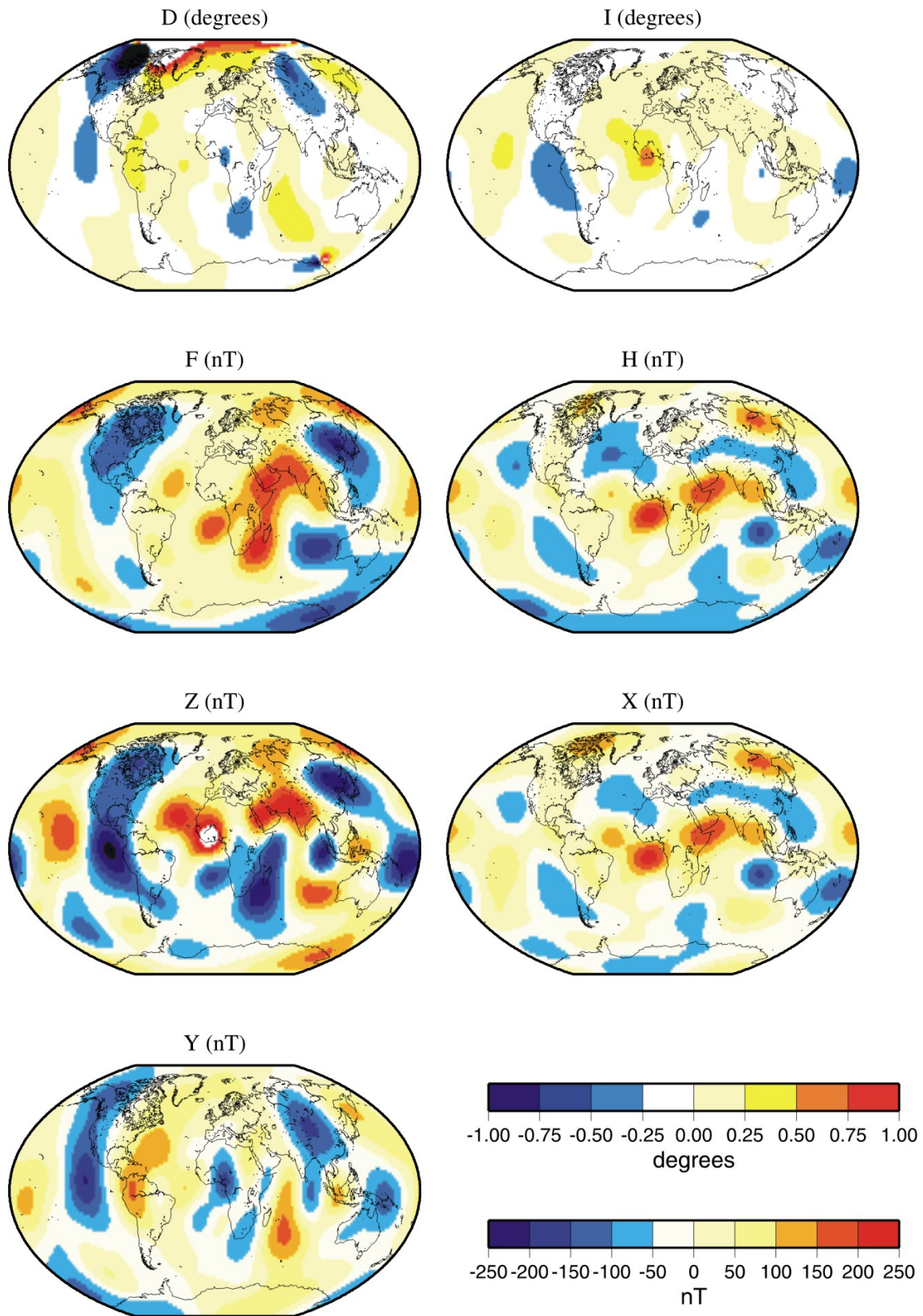


Figure 11: Differences between WMM2005 and WMM2000 at 2005.0 at the Earth's surface.

## 5.5. Model limitations

It is important to recognize that the WMM geomagnetic model and the charts produced from this model characterize only that portion of the Earth's magnetic field that is generated by dynamo action in the Earth's fluid outer core ( $\mathbf{B}_m$ ). The portions of the geomagnetic field generated by the Earth's crust and upper mantle ( $\mathbf{B}_c$ ), and by the ionosphere and magnetosphere ( $\mathbf{B}_d$ ), are not represented in the WMM. Consequently, a magnetic sensor such as a compass or magnetometer may observe spatial and temporal magnetic anomalies when referenced to the WMM. In particular, certain local, regional, and temporal magnetic declination anomalies can exceed 10 degrees. Anomalies of this magnitude are not common but they do exist. Declination anomalies of the order of 3 or 4 degrees are not uncommon but are of small spatial extent and are relatively isolated.

On land, spatial anomalies are produced by mountain ranges, ore deposits, ground struck by lightning, geological faults, and cultural features such as trains, planes, tanks, railroad tracks, power lines, etc. The corresponding deviations are usually smaller at sea, and decrease with increasing altitude of an aircraft or spacecraft. In ocean areas, these anomalies occur most frequently along continental margins, near seamounts, and near ocean ridges, trenches, and fault zones, particularly those of volcanic origin. Ships and submarines are also sources of magnetic anomalies in the ocean.

The crustal contributions could be included in an extended model, expanded to high degrees, as is common for modern gravity field models, such as EGM96 (Lemoine et al., 1998). Since the crustal field is almost constant in time, it can be inferred from all available marine, aeromagnetic, and high resolution CHAMP and future SWARM satellite data, measured at all times. However, this extended model would differ significantly in format from the current WMM, requiring changes in supporting software.

## 6. Test values

Table 6 contains a suite of test values for use in confirming software output. The results are presented for all seven magnetic components for both the main field and secular variation (SV). The area covered is from 80°north to 80°south latitude at 40° intervals and for 0° to 360° east longitude at 60° intervals. Results for *D* and *I* are shown in units of decimal degrees for the main field and units of minutes per year for the secular variation. Results for *H*, *X*, *Y*, *Z*, and *F* are shown in nT for the main field and in nT/year for the secular variation. Declination is considered positive east, inclination and vertical component are considered positive down.

**Table 6: Test results for the World Magnetic Model 2005**

Date: 2007.50 Altitude: 0.0 km geodetic								
Lat	Long	<i>D</i>	<i>I</i>	<i>H</i>	<i>X</i>	<i>Y</i>	<i>Z</i>	<i>F</i>
80.0	0.0	-6.92	82.95	6722	6673	-810	54370	54784
	SV:	25	0	1	7	48	54	54
80.0	60.0	35.84	84.80	5154	4178	3018	56671	56905
	SV:	13	1	-10	-19	9	61	60
80.0	120.0	0.55	87.69	2362	2362	23	58638	58686
	SV:	-12	0	-3	-3	-8	60	60
80.0	180.0	8.65	85.76	4274	4226	643	57609	57768
	SV:	-27	1	-9	-4	-34	69	68
80.0	240.0	31.25	88.79	1215	1038	630	57475	57488
	SV:	-198	-2	26	59	-46	38	39
80.0	300.0	-54.44	85.59	4306	2504	-3503	55862	56028
	SV:	59	-1	14	68	32	31	32
40.0	0.0	-0.98	55.05	25572	25568	-436	36584	44635
	SV:	6	0	17	18	47	24	30
40.0	60.0	5.08	59.24	26012	25910	2303	43711	50865
	SV:	4	4	-14	-17	27	88	68
40.0	120.0	-7.40	57.90	28532	28294	-3676	45491	53699
	SV:	-6	-1	-3	-9	-45	-30	-27
40.0	180.0	5.79	52.92	25299	25170	2553	33470	41956
	SV:	-2	-1	27	28	-13	20	32
40.0	240.0	14.75	63.72	22591	21846	5753	45752	51025
	SV:	-7	-1	-23	-11	-51	-76	-79
40.0	300.0	-17.79	63.45	22170	21110	-6772	44377	49607
	SV:	8	-6	34	48	39	-126	-98
0.0	0.0	-6.44	-28.75	27681	27506	-3106	-15186	31573
	SV:	7	-5	6	12	52	-51	30
0.0	60.0	-4.13	-17.41	35319	35228	-2544	-11072	37014
	SV:	3	6	80	82	23	44	63
0.0	120.0	1.08	-16.91	39427	39420	741	-11986	41208
	SV:	-2	1	-3	-3	-21	12	-7
0.0	180.0	9.62	-4.85	34130	33650	5706	-2894	34252
	SV:	-1	-2	-21	-20	-9	-22	-19
0.0	240.0	9.13	9.45	30654	30265	4865	5105	31076
	SV:	-2	1	-38	-34	-27	5	-36
0.0	300.0	-14.63	15.79	26962	26089	-6808	7623	28019
	SV:	-6	-15	-30	-41	-38	-135	-66
-40.0	0.0	-23.43	-65.09	10472	9608	-4164	-22544	24858
	SV:	1	-3	-45	-39	22	44	-59
-40.0	60.0	-45.31	-64.40	17953	12626	-12764	-37478	41556

	<b>SV:</b>	-5	-6	-27	-36	2	-113	91
<b>-40.0</b>	<b>120.0</b>	-3.36	-73.44	17712	17681	-1037	-59562	62139
	<b>SV:</b>	2	1	2	3	11	36	-34
<b>-40.0</b>	<b>180.0</b>	21.80	-64.40	23516	21835	8732	-49090	54432
	<b>SV:</b>	3	0	-18	-23	11	38	-42
<b>-40.0</b>	<b>240.0</b>	22.46	-52.65	24594	22728	9397	-32230	40541
	<b>SV:</b>	1	1	-41	-41	-9	64	-76
<b>-40.0</b>	<b>300.0</b>	-2.65	-41.52	18339	18319	-849	-16236	24494
	<b>SV:</b>	-8	-7	-62	-64	-40	-9	-41
<b>-80.0</b>	<b>0.0</b>	-21.77	-66.03	19146	17781	-7101	-43062	47127
	<b>SV:</b>	-5	2	-4	-14	-23	68	-64
<b>-80.0</b>	<b>60.0</b>	-74.33	-70.24	17800	4808	-17139	-49562	52662
	<b>SV:</b>	-8	1	3	-38	-14	44	-41
<b>-80.0</b>	<b>120.0</b>	-140.75	-77.70	12874	-9970	-8146	-59046	60433
	<b>SV:</b>	-10	1	10	-30	22	37	-34
<b>-80.0</b>	<b>180.0</b>	131.56	-78.88	11846	-7858	8865	-60295	61448
	<b>SV:</b>	-7	2	26	2	36	60	-54
<b>-80.0</b>	<b>240.0</b>	70.39	-72.71	16692	5601	15724	-53637	56175
	<b>SV:</b>	-4	2	10	24	2	85	-78
<b>-80.0</b>	<b>300.0</b>	23.86	-67.02	19271	17624	7796	-45453	49370
	<b>SV:</b>	-4	1	-11	-2	-24	80	-78

## 7. Contacts

The model, associated software, digital charts, and documentation are available via the Web at <http://www.ngdc.noaa.gov/seg/WMM/> or by contacting NGDC, BGS, or NGA.

### Model and Software Support

National Geophysical Data Center  
NOAA E/GC 2  
325 Broadway  
Boulder, CO 80305-3328  
USA  
Attention: Susan McLean or Stefan Maus  
Phone: + (303) 497-6478 or -6522  
Email: [Susan.McLean@noaa.gov](mailto:Susan.McLean@noaa.gov) or [Stefan.Maus@noaa.gov](mailto:Stefan.Maus@noaa.gov)  
Web: <http://www.ngdc.noaa.gov/seg/WMM/>

British Geological Survey  
Murchison House  
West Mains Road  
Edinburgh, EH9 3LA  
UK  
Attention: Susan Macmillan or Vincent Lesur  
Phone: + 44 131 667 1000  
Email: [smac@bgs.ac.uk](mailto:smac@bgs.ac.uk) or [vbfl@bgs.ac.uk](mailto:vbfl@bgs.ac.uk)  
Web: <http://www.geomag.bgs.ac.uk/navigation.html>

Applicability within the U.S. Department of Defense

National Geospatial-Intelligence Agency	
PRG / CSAT, M.S. L-41	IB MS L-64
3838 Vogel Road	3838 Vogel Road
Arnold, Mo 63010	Arnold, Mo 63010
USA	USA
Attention: Craig Rollins	Attention: Scott True
Email: <a href="mailto:Craig.M.Rollins@nga.mil">Craig.M.Rollins@nga.mil</a>	Email: <a href="mailto:Scott.A.True@nga.mil">Scott.A.True@nga.mil</a>

### **Acknowledgements**

The overall coordination and production of the joint US/UK World Magnetic Model for the 2005 Epoch (WMM-2005) was the responsibility of Susan McLean of the National Geophysical Data Center (NGDC) and Susan Macmillan of the British Geological Survey (BGS). This work was done under the sponsorship of the U.S. National Geospatial-Intelligence Agency (NGA) and the UK Ministry of Defence through the Defence Geographic Imagery and Intelligence Agency (DGIA). In addition, Stefan Maus (NGDC/CIRES), Vincent Lesur (BGS), and Alan Thomson (BGS) contributed to the data selection, quality control, model development, model review, and the final Report. David Dater, Courtney Hoskins, and Joy Ikelman (NGDC) contributed graphics and reviewed the Report. The Danish Meteorological Institute, supported by the Danish Space Research Institute and the Ministries of Trade, Research and Transport operates the Ørsted satellite mission and data center. The CHAMP mission and data center is operated by GeoForschungsZentrum Potsdam, Germany, supported by the German Aerospace Center (DLR) and by the Federal Ministry of Education and Research (BMBF). The INTERMAGNET program provides valuable support and resources, which help the numerous unnamed individuals from many countries, private institutions, and government agencies around the world that collect and process magnetic field data at geomagnetic observatories worldwide, and kindly contributed data essential for the development of the WMM. In addition, observatory data and magnetic indices were provided by the World Data Centers in Copenhagen, Edinburgh, and Boulder. This model could not have been produced without the efforts of all of these individuals and institutes.

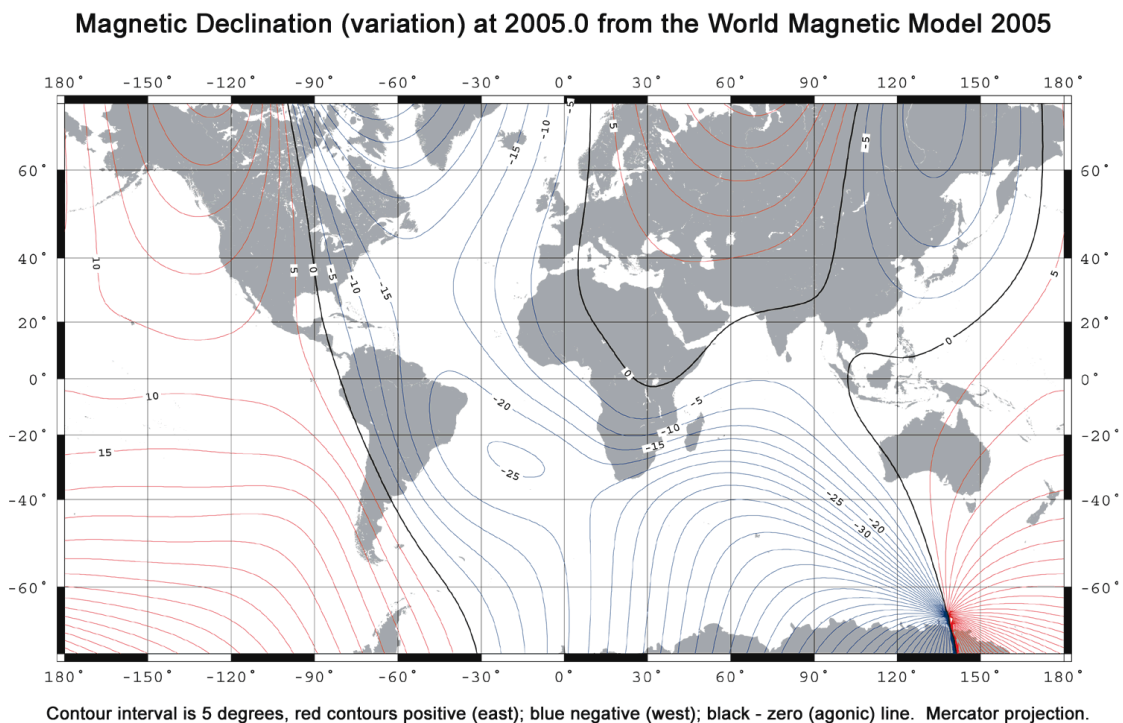
## Maps

All of the charts are available in digital PDF format on the CD-ROM or from the WMM web <http://www.ngdc.noaa.gov/seg/WMM/>. The Mercator charts are approximately 48 inches wide and 36 inches high, but can be printed on various paper sizes using the “fit to paper” option.

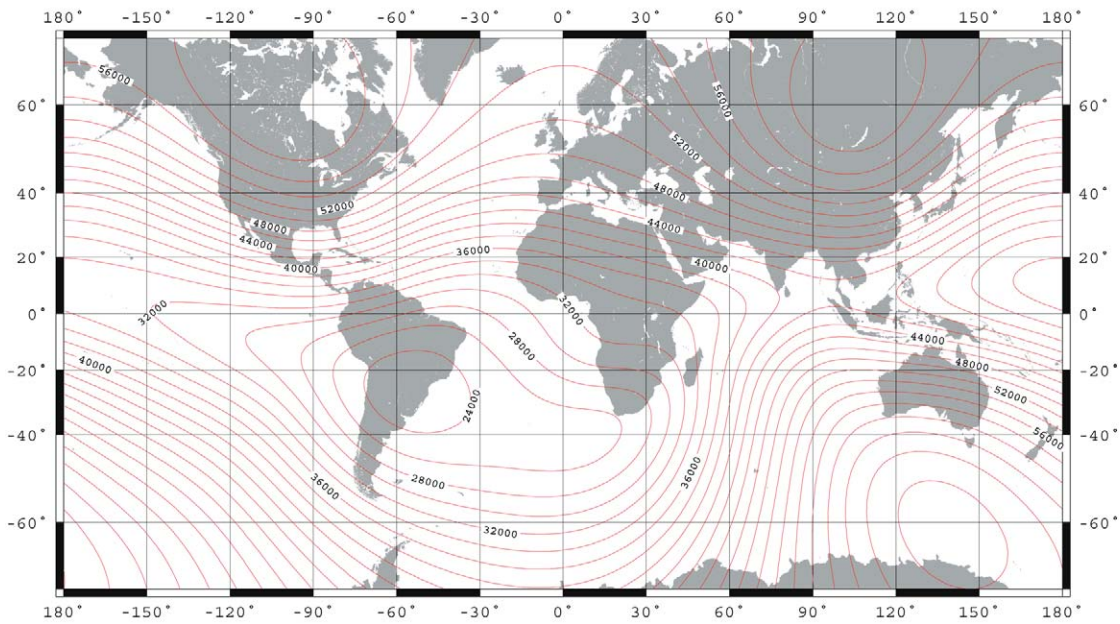
The following charts are available:

- World Mercator projection for the Main Field – Elements *D, F, H, I, X, Y,* and *Z.*
- North/South Polar Stereographic Projection of the Main Field – Elements *D, F, H, I, X, Y,* and *Z.*
- World Mercator projection for the Secular Variation Field – Elements *D, F, H, I, X, Y,* and *Z.*
- North/South Polar Stereographic Projection of the Secular Variation Field – Elements *D, F, H, I, X, Y,* and *Z.*
- North/South Polar Stereographic Projection of Grid Variation (GV)

Main field maps: Mercator Projection

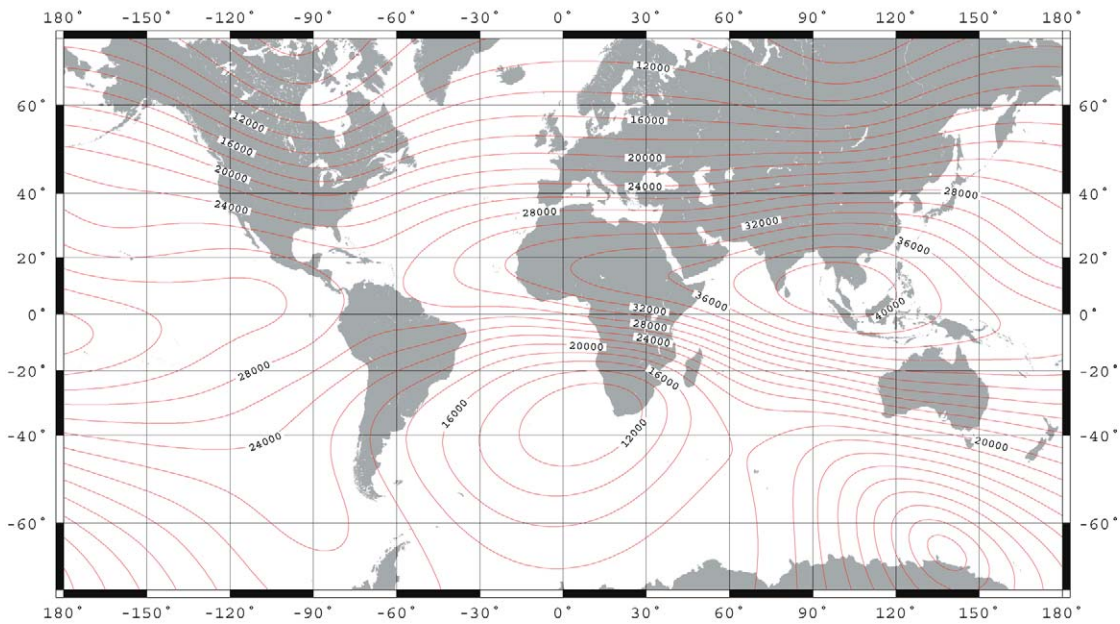


### Magnetic Total Intensity (F) at 2005.0 from the World Magnetic Model 2005



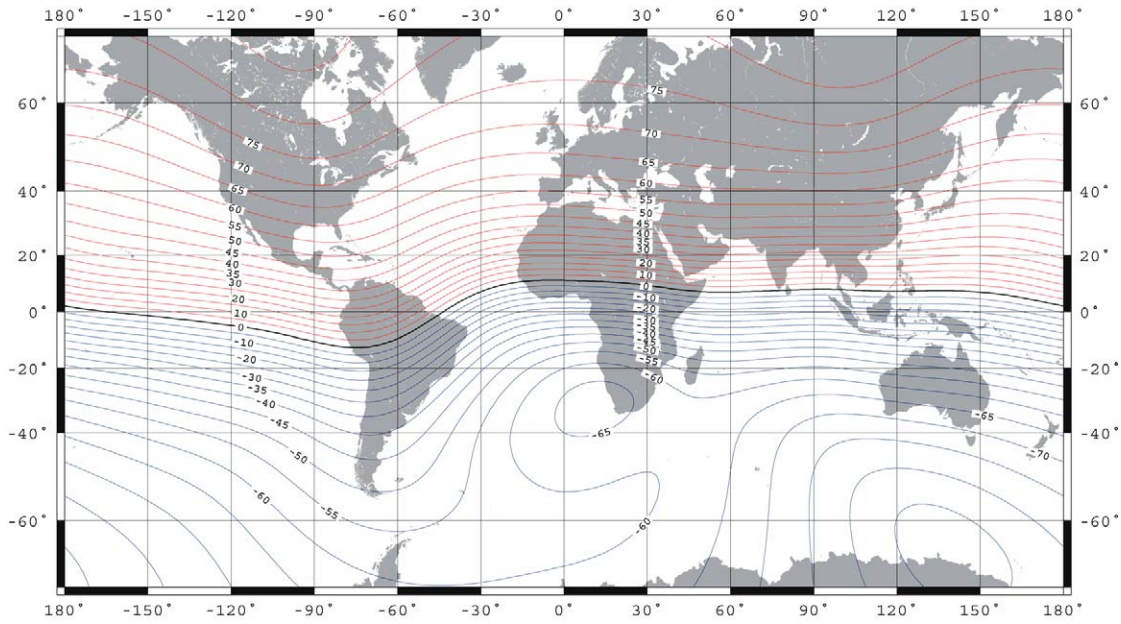
Contour interval is 2000 nT. Mercator projection.

### Magnetic Horizontal Intensity (H) at 2005.0 from the World Magnetic Model 2005



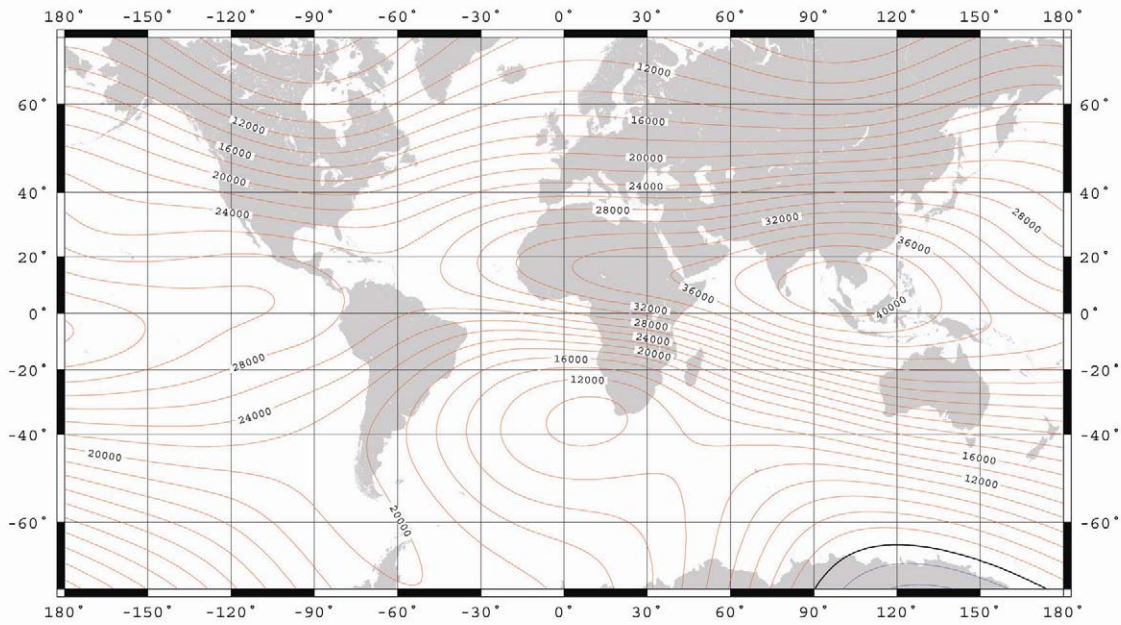
Contour interval is 2000 nT. Mercator projection.

### Magnetic Inclination (I) at 2005.0 from the World Magnetic Model 2005



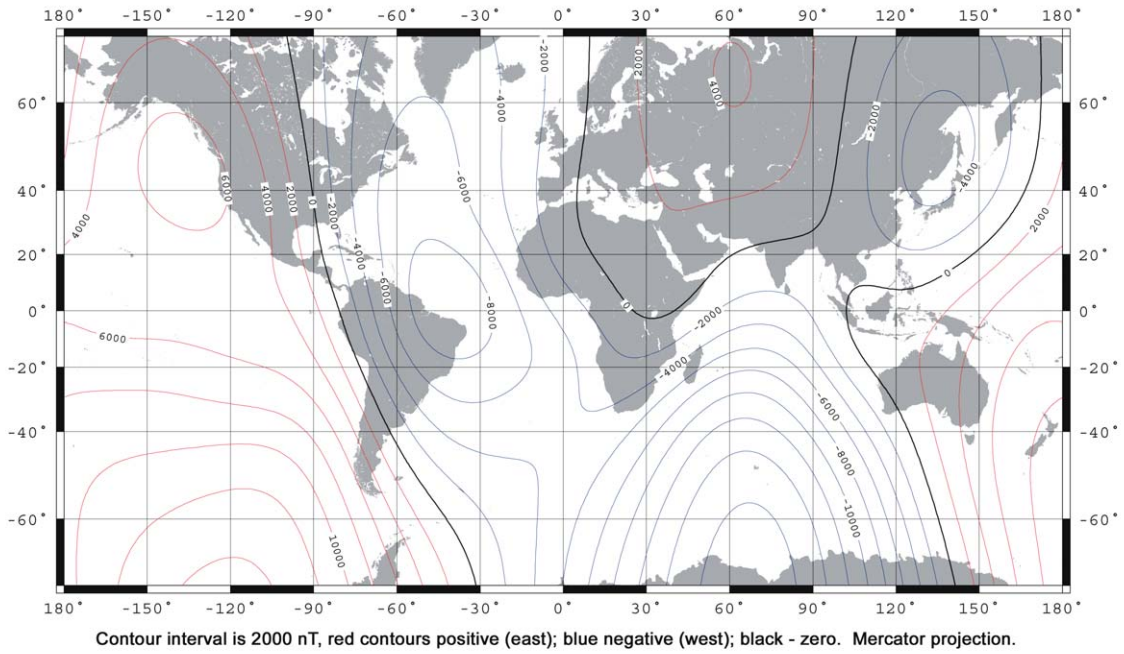
Contour interval is 5 degrees, red contours positive (down); blue negative (up); black - zero (agonic) line. Mercator projection.

### Magnetic North Component (X) at 2005.0 from the World Magnetic Model 2005

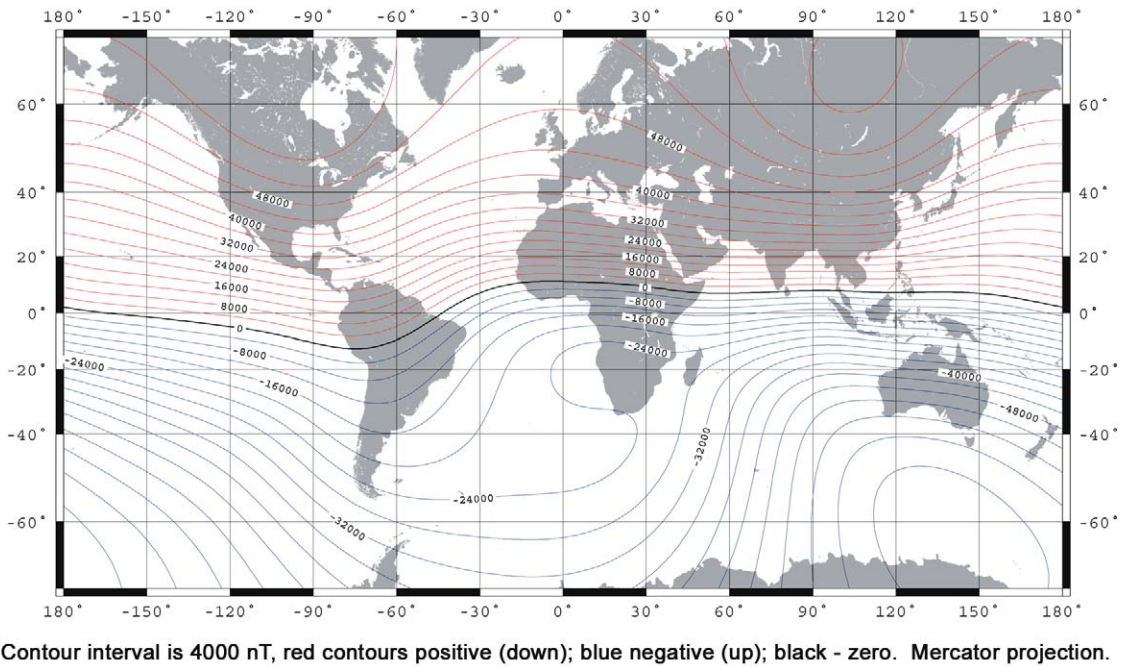


Contour interval is 2000 nT, red contours positive (north); blue negative (south); black - zero. Mercator projection.

### Magnetic East Component (Y) at 2005.0 from the World Magnetic Model 2005

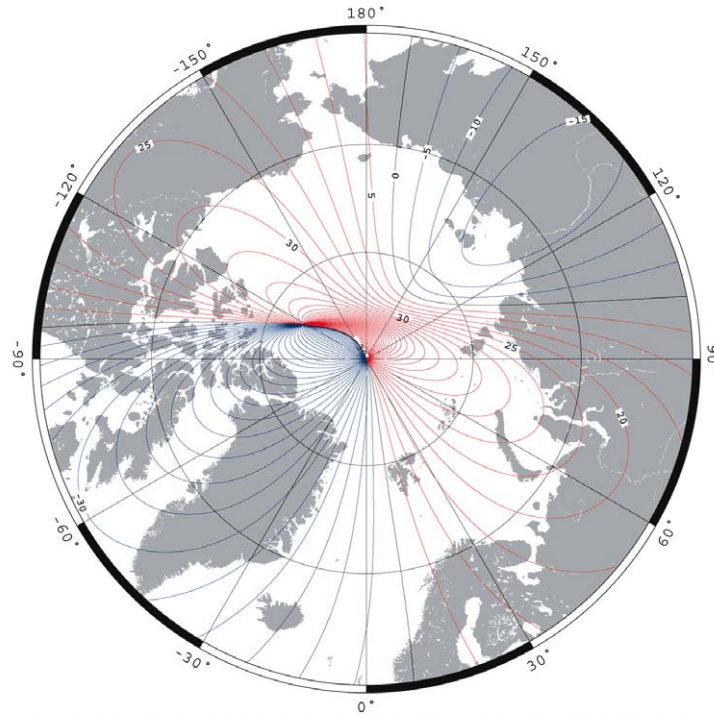


### Magnetic Vertical Intensity (Z) at 2005.0 from the World Magnetic Model 2005



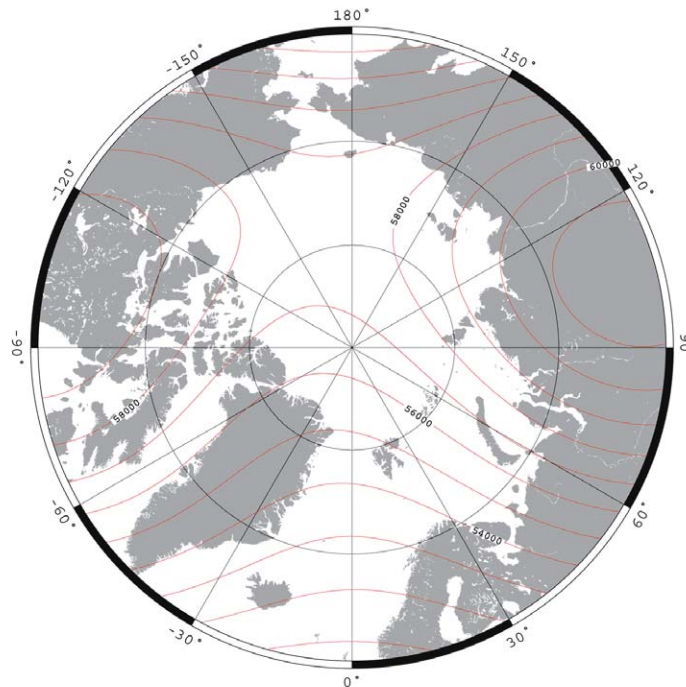
## Main field maps: North Polar Stereographic Projection

Magnetic Declination (D) at 2005.0 from the World Magnetic Model 2005



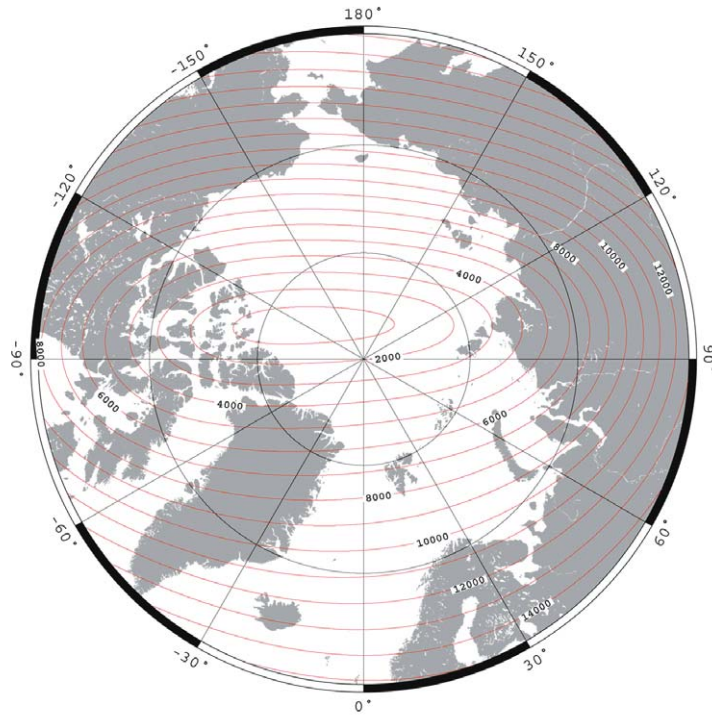
Contour interval is 5 degrees, red contours positive (east), blue negative (west), black - zero. North polar region. Polar Stereographic Projection.

Total Intensity (F) at 2005.0 from the World Magnetic Model 2005



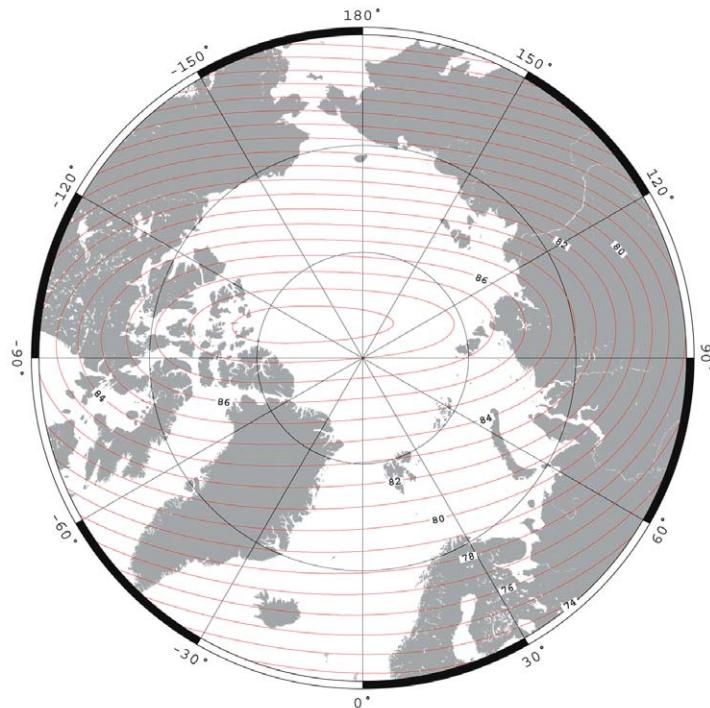
North polar region. Contour interval is 1000 nT. Polar Stereographic Projection.

Horizontal Intensity (H) at 2005.0 from the World Magnetic Model 2005



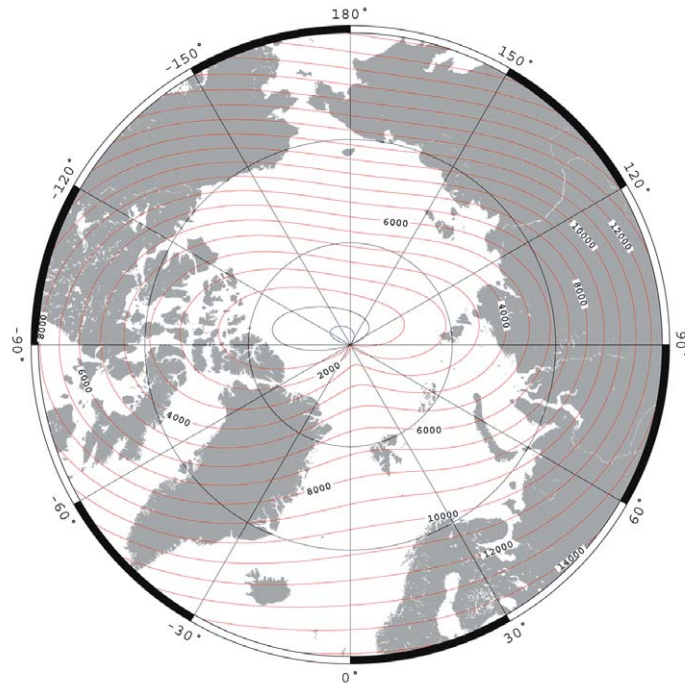
North polar region. Contour interval is 1000 nT. Polar Stereographic Projection.

Magnetic Inclination (I) at 2005.0 from the World Magnetic Model 2005



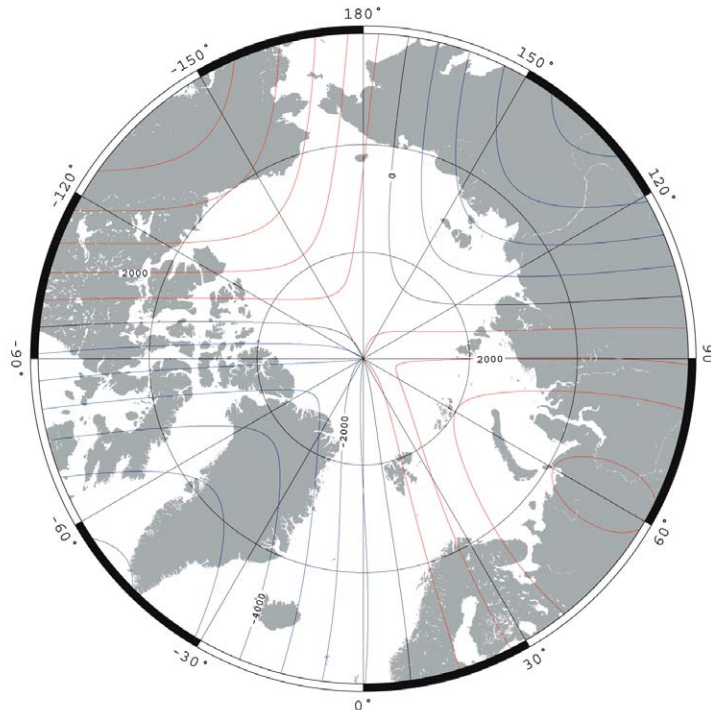
North polar region. Contour interval is 1 degree. Polar Stereographic Projection.

North Component (X) at 2005.0 from the World Magnetic Model 2005



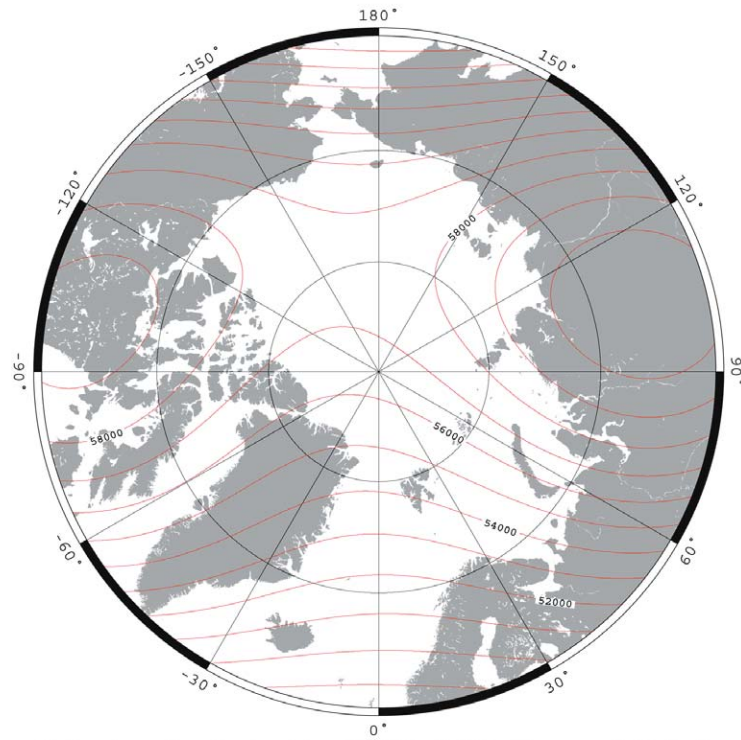
North polar region. Contour interval is 1000 nT, red positive (north), blue negative (south), black - zero. Polar Stereographic Projection.

East Component (Y) at 2005.0 from the World Magnetic Model 2005



North polar region. Contour interval is 1000 nT, red positive (east), blue negative (west), black - zero. Polar Stereographic Projection.

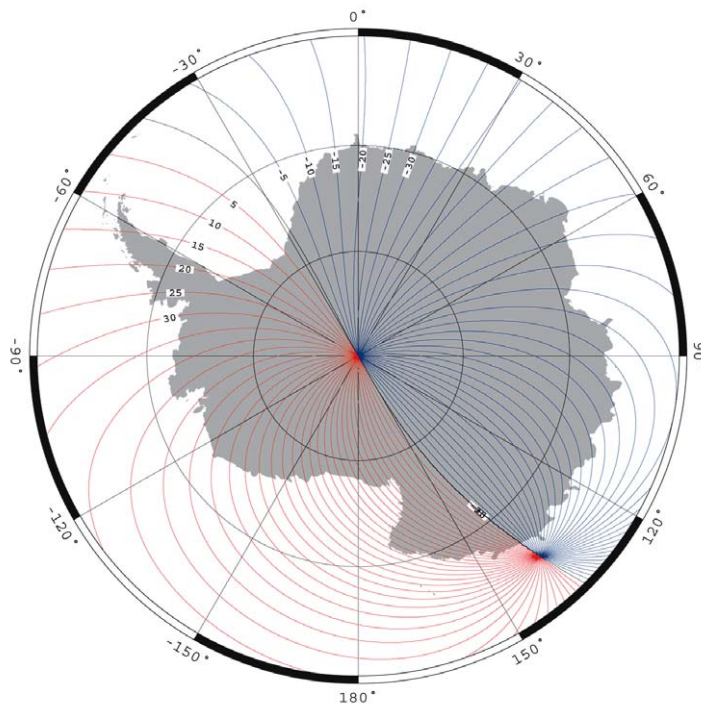
Vertical Component (Z) at 2005.0 from the World Magnetic Model 2005



North polar region. Contour interval is 1000 nT. Polar Stereographic Projection.

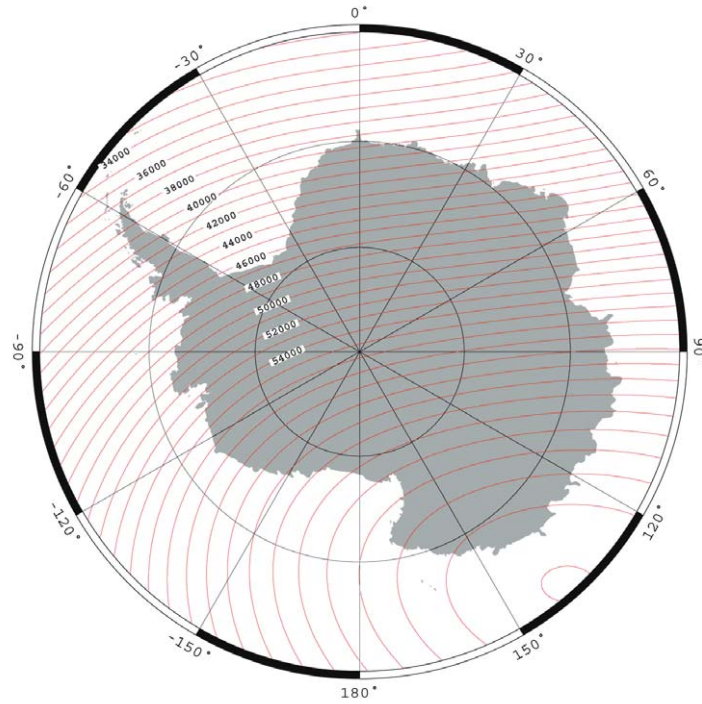
### Main field maps: South Polar Stereographic Projection

Magnetic Declination (D) at 2005.0 from the World Magnetic Model 2005



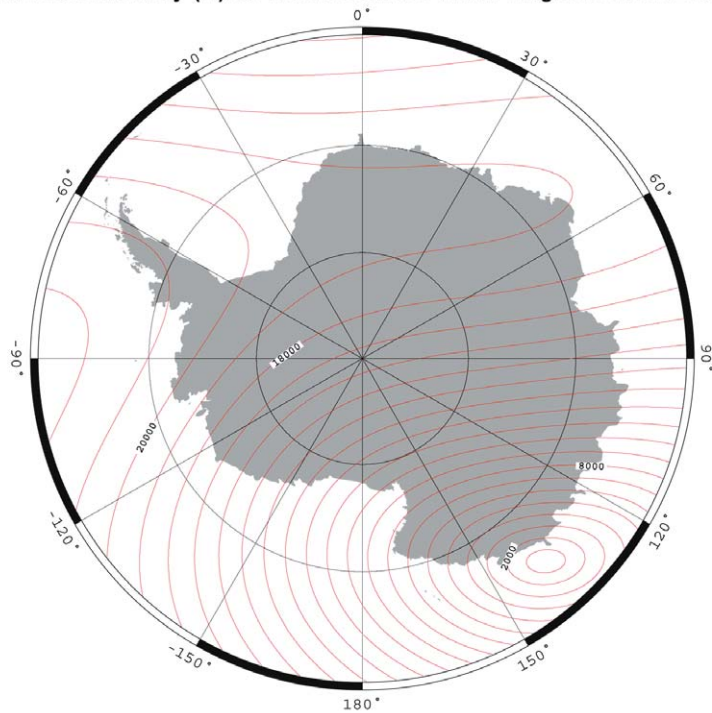
Contour interval is 5 degrees, red contours positive (east), blue negative (west), black - zero. South polar region. Polar Stereographic Projection.

Total Intensity (F) at 2005.0 from the World Magnetic Model 2005



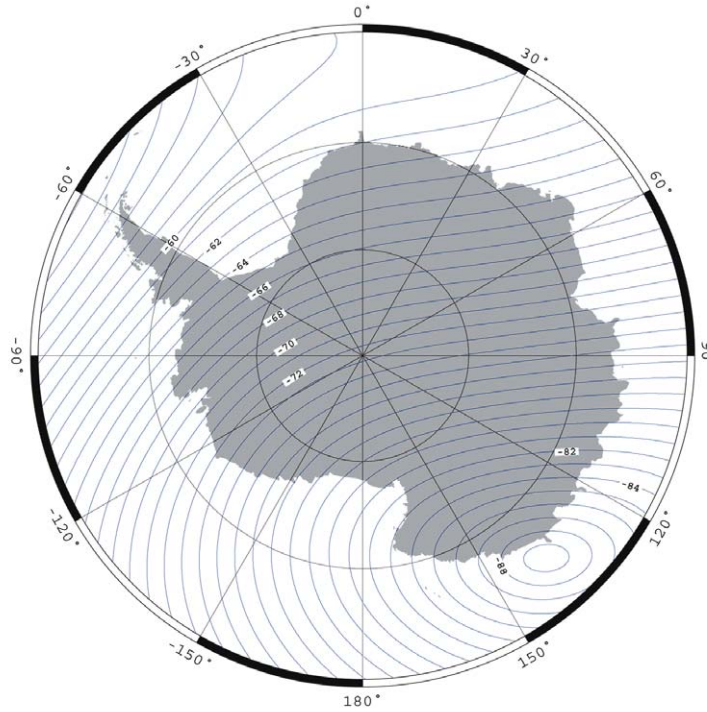
South polar region. Contour interval is 1000 nT. Polar Stereographic Projection.

Horizontal Intensity (H) at 2005.0 from the World Magnetic Model 2005



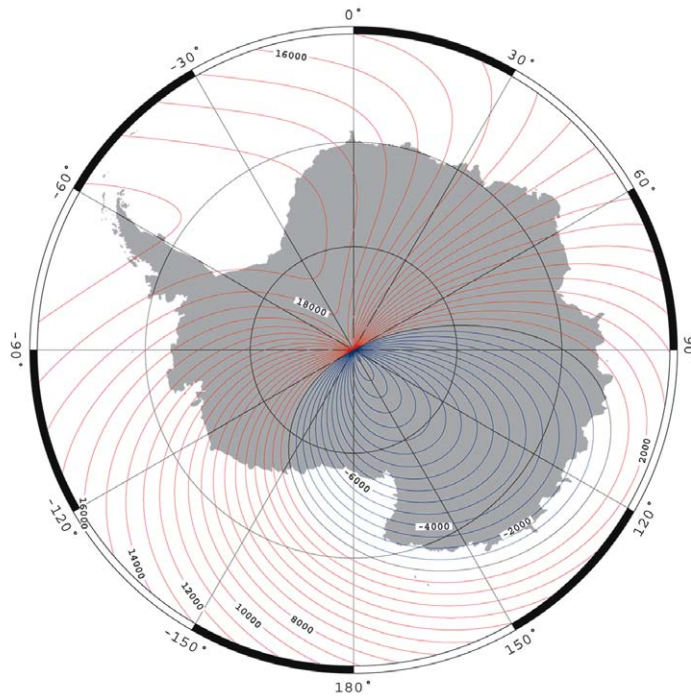
South polar region. Contour interval is 1000 nT. Polar Stereographic Projection.

Magnetic Inclination (I) at 2005.0 from the World Magnetic Model 2005



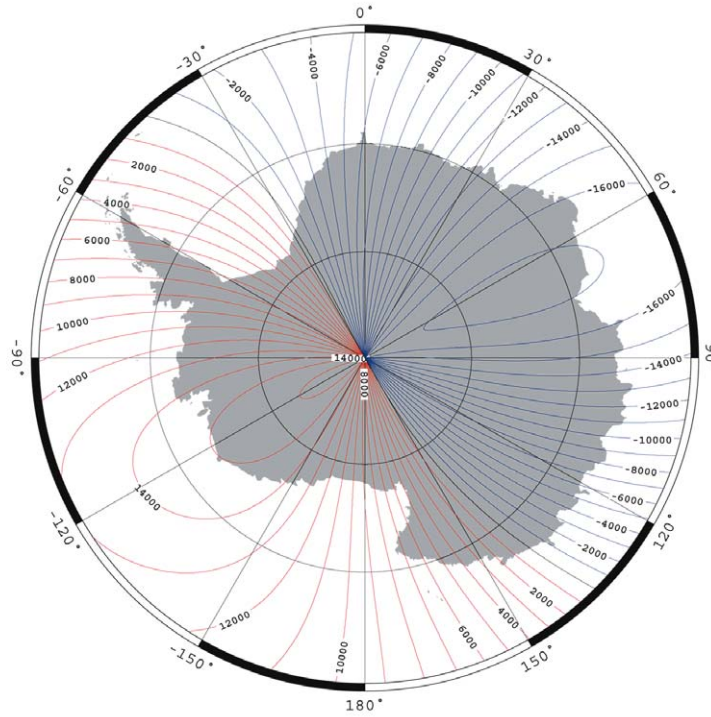
South polar region. Contour interval is 1 degree. Polar Stereographic Projection.

North Component (X) at 2005.0 from the World Magnetic Model 2005



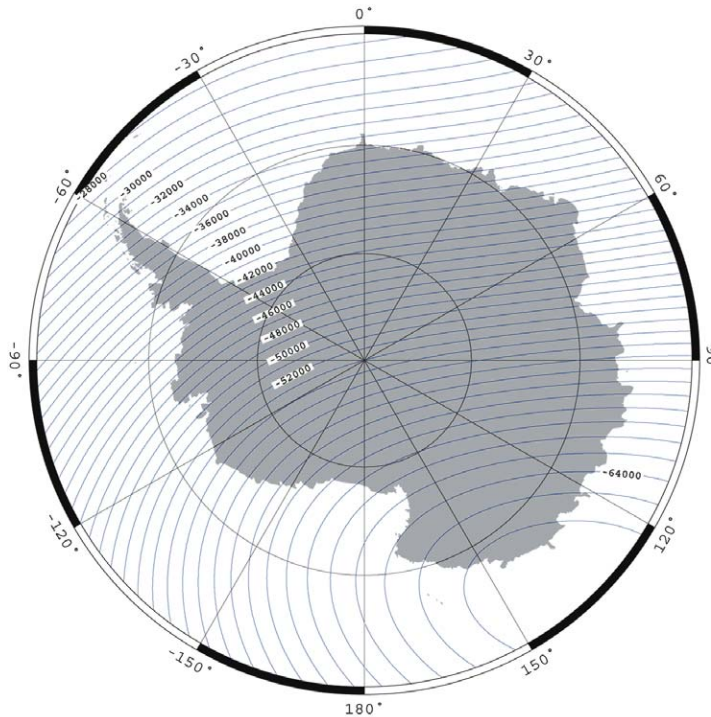
South polar region. Contour interval is 1000 nT, red positive (north), blue negative (south), black - zero. Polar Stereographic Projection.

East Component (Y) at 2005.0 from the World Magnetic Model 2005



South polar region. Contour interval is 1000 nT, red positive (east), blue negative (west), black - zero. Polar Stereographic Projection.

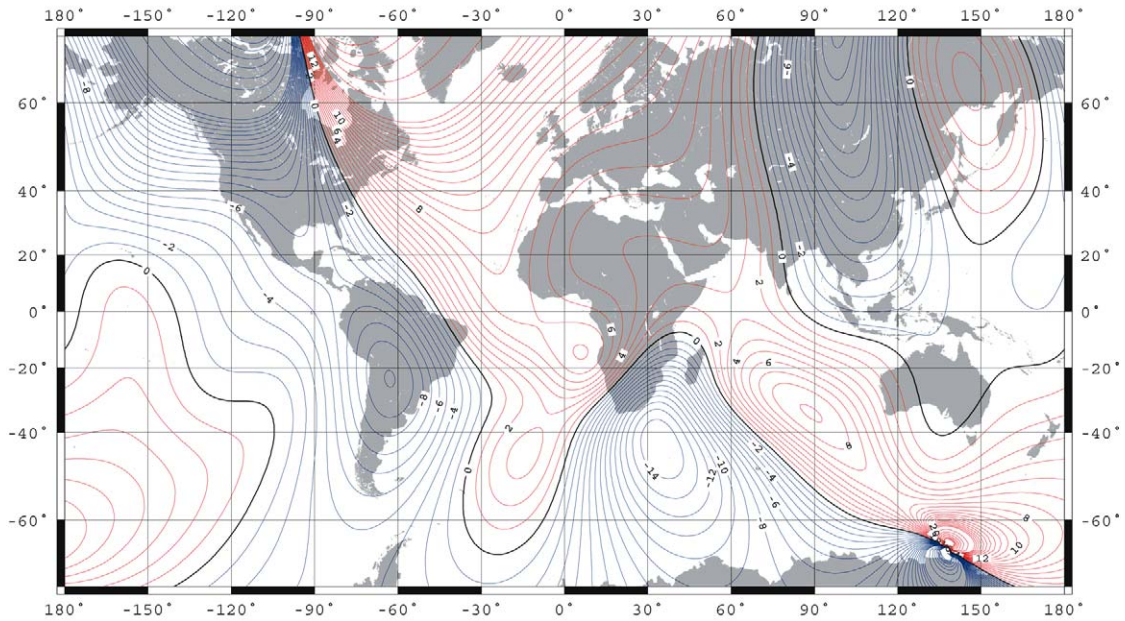
Vertical Component (Z) at 2005.0 from the World Magnetic Model 2005



South polar region. Contour interval is 1000 nT. Polar Stereographic Projection.

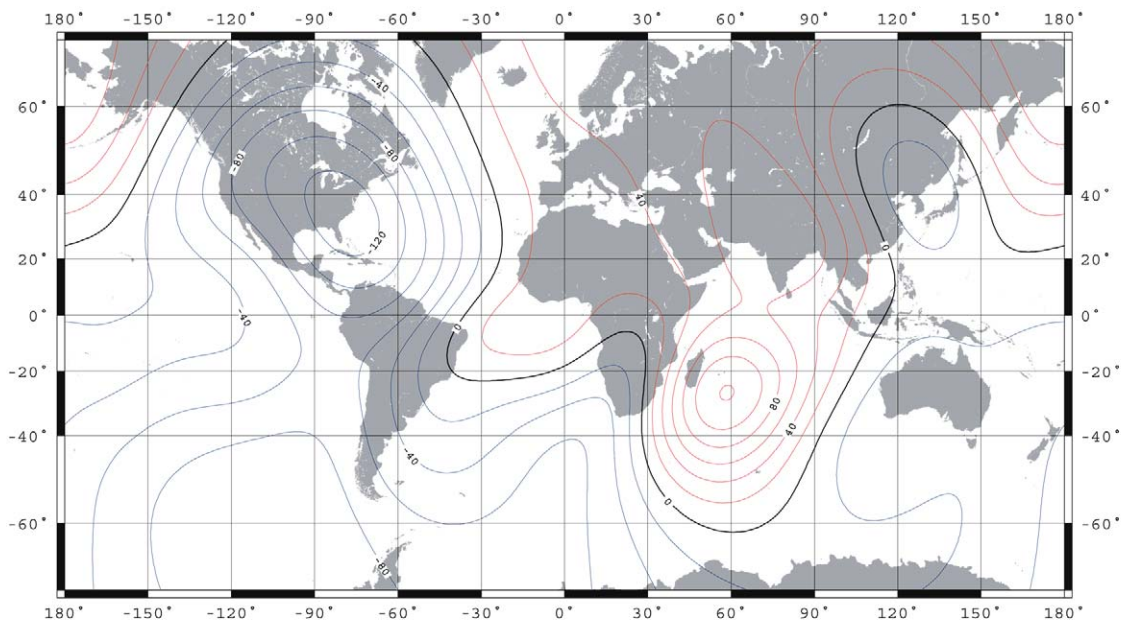
Secular variation maps: Mercator Projection

**Annual Rate of Change of Magnetic Declination (D)  
for 2005-2010 from the World Magnetic Model 2005**



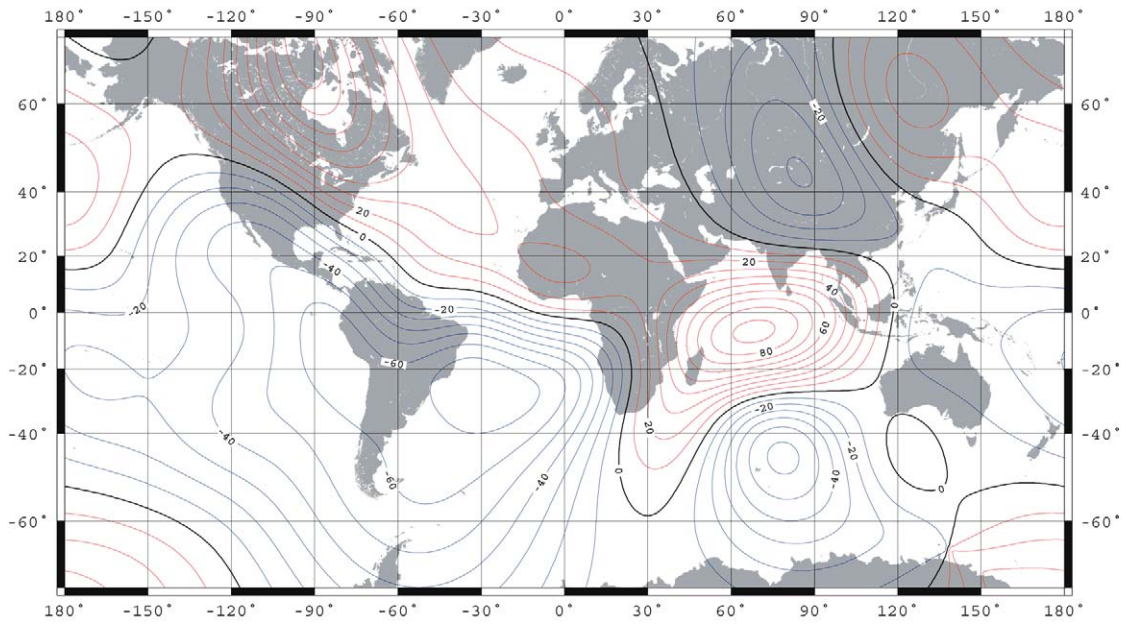
Contour interval is 1' / year up to  $\pm 20'$  / year, 5' / year thereafter, red contours easterly change; blue westerly change; black zero change. Mercator projection.

**Annual Rate of Change of Magnetic Total Intensity (F)  
for 2005-2010 from the World Magnetic Model 2005**



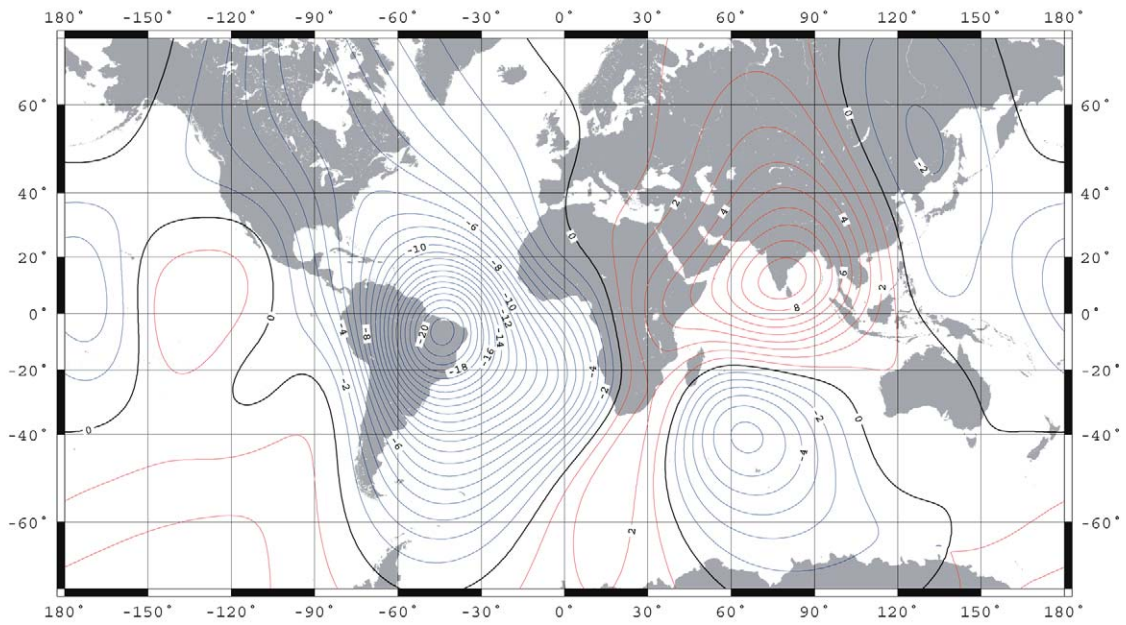
Contour interval is 20 nT/year, red contours positive change; blue negative; black zero change. Mercator projection.

### Annual Rate of Change of Magnetic Horizontal Intensity (H) for 2005-2010 from the World Magnetic Model 2005



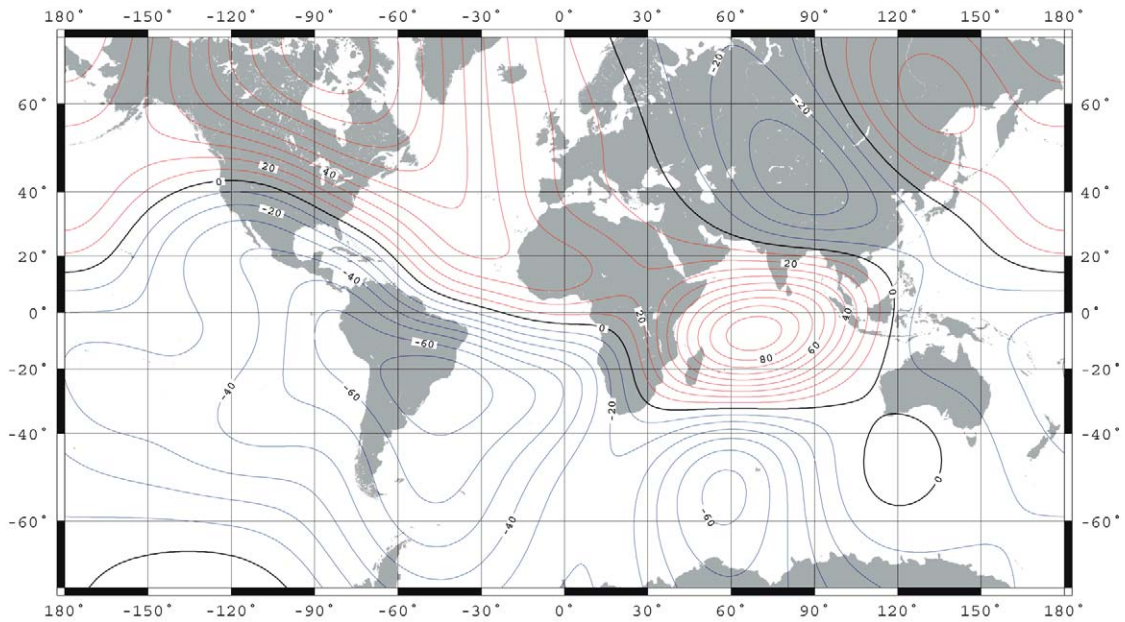
Contour interval is 10 nT/year, red contours positive change; blue negative; black zero change. Mercator projection.

### Annual Rate of Change of Magnetic Inclination (I) for 2005-2010 from the World Magnetic Model 2005



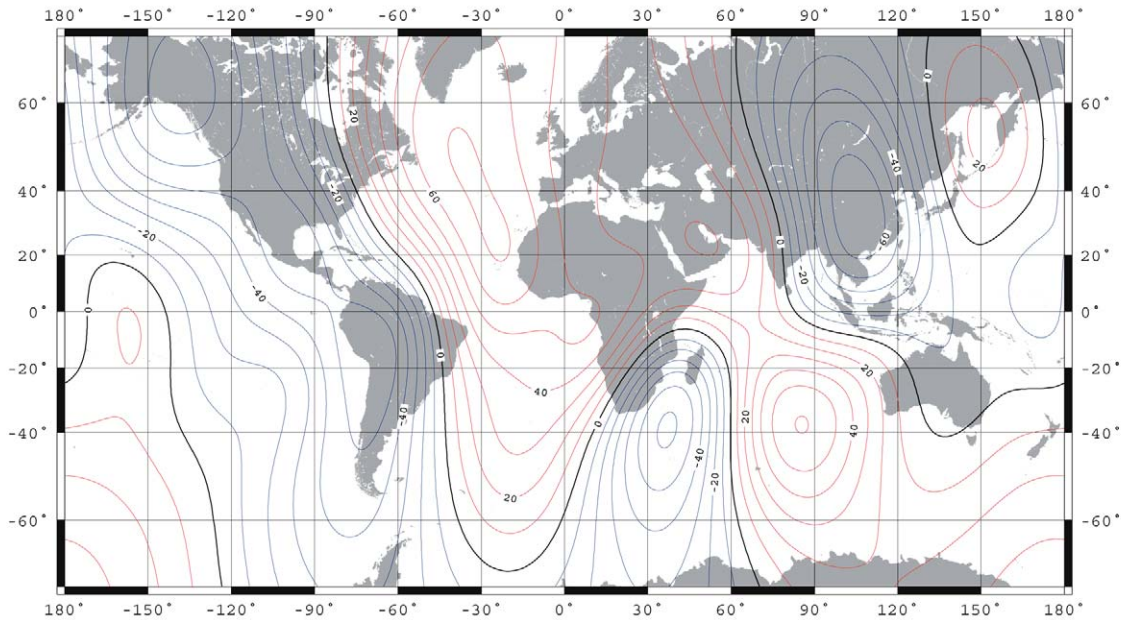
Contour interval is 1' / year, red contours positive (down); blue negative (up); black zero change. Mercator projection.

### Annual Rate of Change of Magnetic North Component (X) for 2005-2010 from the World Magnetic Model 2005



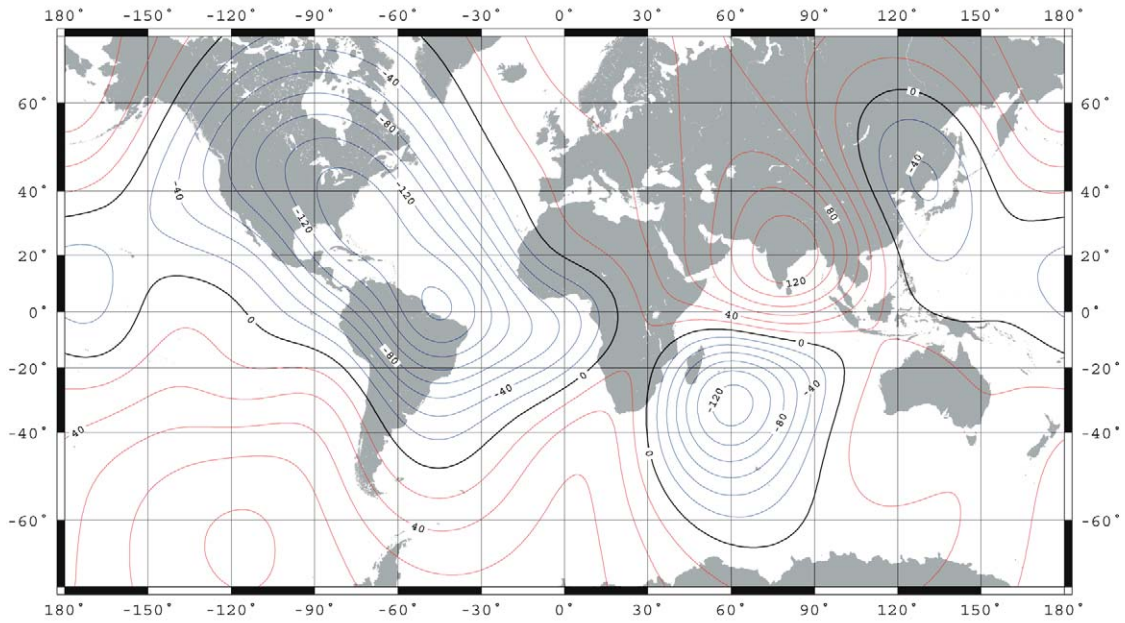
Contour interval is 10 nT/year, red contours positive change; blue negative; black zero change. Mercator projection.

### Annual Rate of Change of Magnetic East Component (Y) for 2005-2010 from the World Magnetic Model 2005



Contour interval is 10 nT/year, red contours positive change; blue negative; black zero change. Mercator projection.

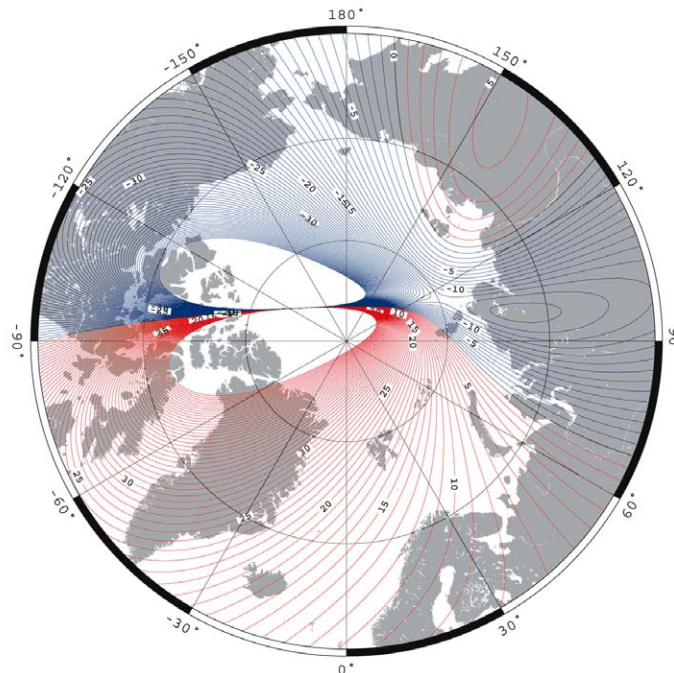
### Annual Rate of Change of Magnetic Vertical Intensity (Z) for 2005-2010 from the World Magnetic Model 2005



Contour interval is 20 nT/year, red contours positive (down) change; blue negative (up); black zero change. Mercator projection.

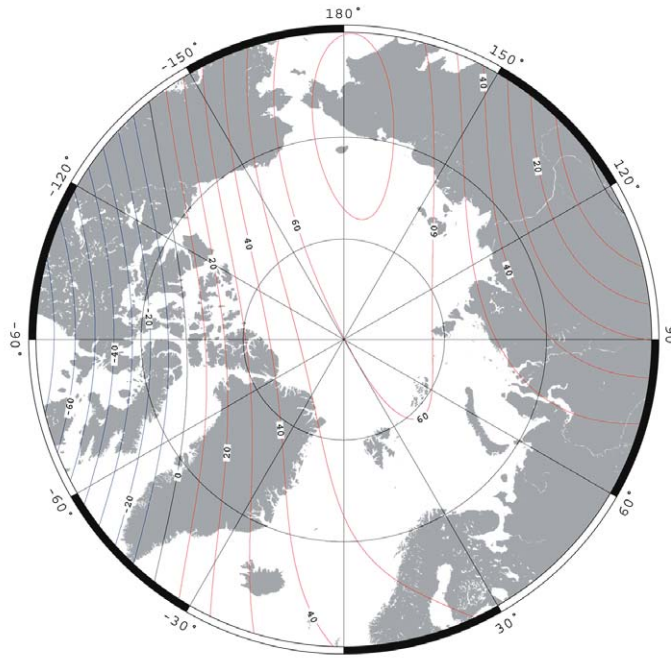
### Secular variation maps: North Polar Stereographic Projection

#### Annual Rate of Change of Magnetic Declination (D) for 2005-2010 from the World Magnetic Model 2005



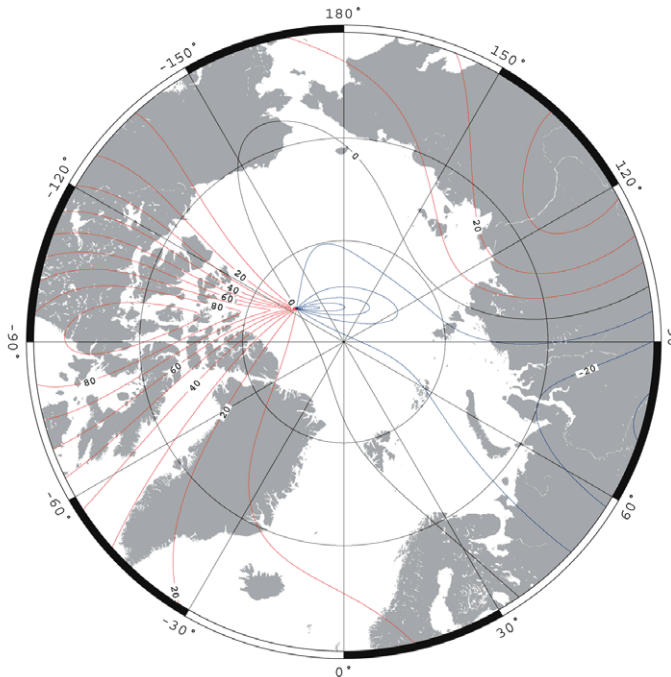
North polar region, contour interval is 1' / year up to 160' / year, red contours easterly change; blue westerly change; black zero change. Polar Stereographic projection.

**Annual Rate of Change of Magnetic Total Intensity (F)  
for 2005-2010 from the World Magnetic Model 2005**



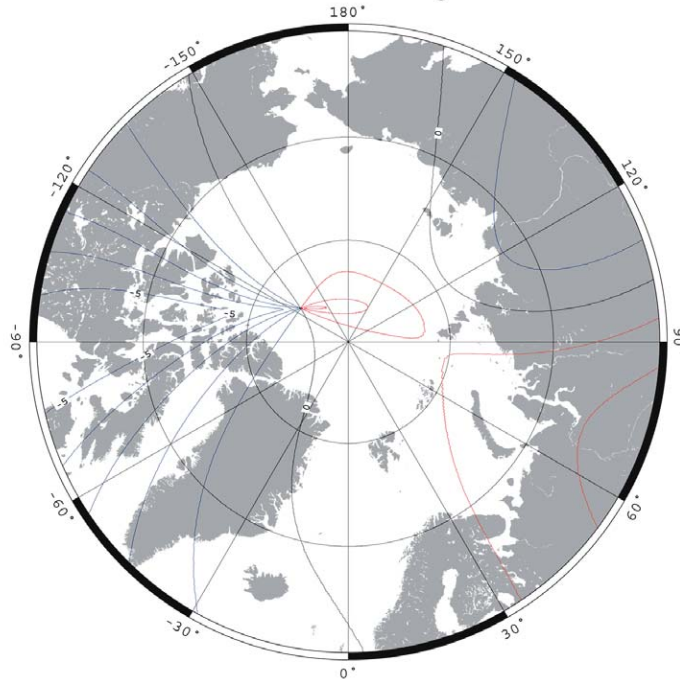
North polar region, contour interval is 10 nT/year,  
red contours positive change; blue negative; black zero change.  
Polar Stereographic projection.

**Annual Rate of Change of Magnetic Horizontal Intensity (H)  
for 2005-2010 from the World Magnetic Model 2005**



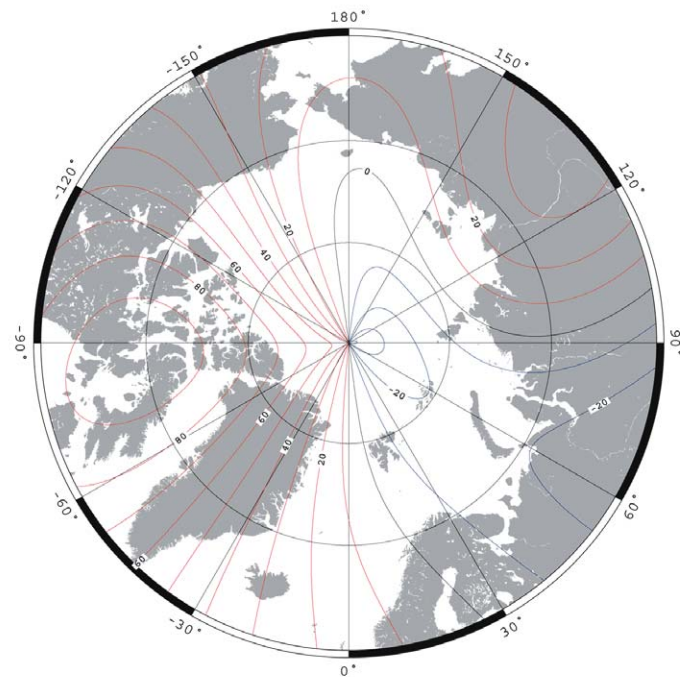
North polar region, contour interval is 10 nT / year,  
red contours positive change; blue negative; black zero  
change. Polar Stereographic projection.

**Annual Rate of Change of Magnetic Inclination (I)  
for 2005-2010 from the World Magnetic Model 2005**



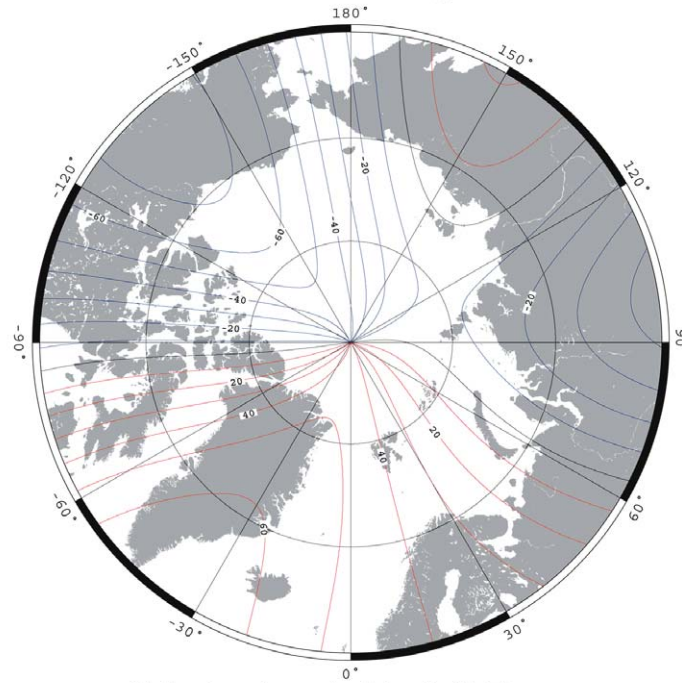
North polar region, contour interval is 1' / year,  
red contours positive change; blue negative; black zero change.  
Polar Stereographic projection.

**Annual Rate of Change of Magnetic North Component (X)  
for 2005-2010 from the World Magnetic Model 2005**



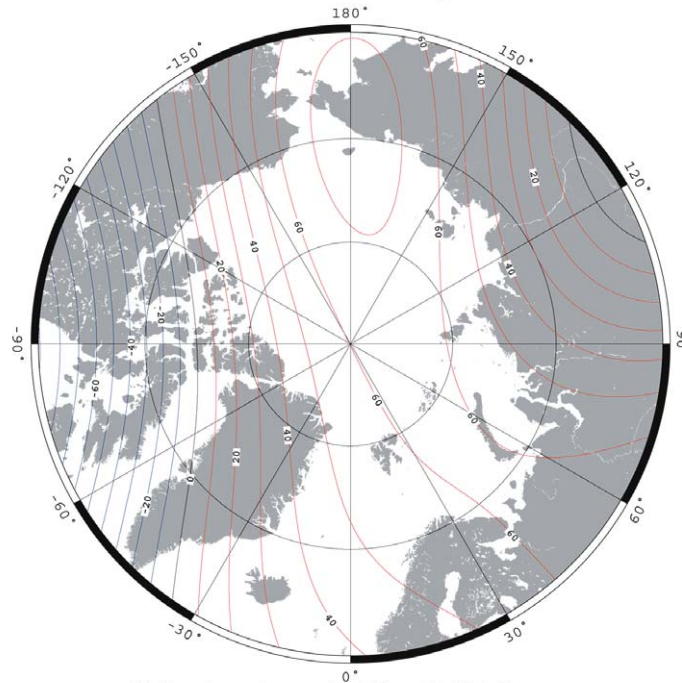
North polar region, contour interval is 10 nT/year,  
red contours positive change; blue negative; black zero change.  
Polar Stereographic projection.

**Annual Rate of Change of Magnetic East Component (Y)  
for 2005-2010 from the World Magnetic Model 2005**



North polar region, contour interval is 10 nT/year,  
red contours positive change; blue negative; black zero change.  
Polar Stereographic projection.

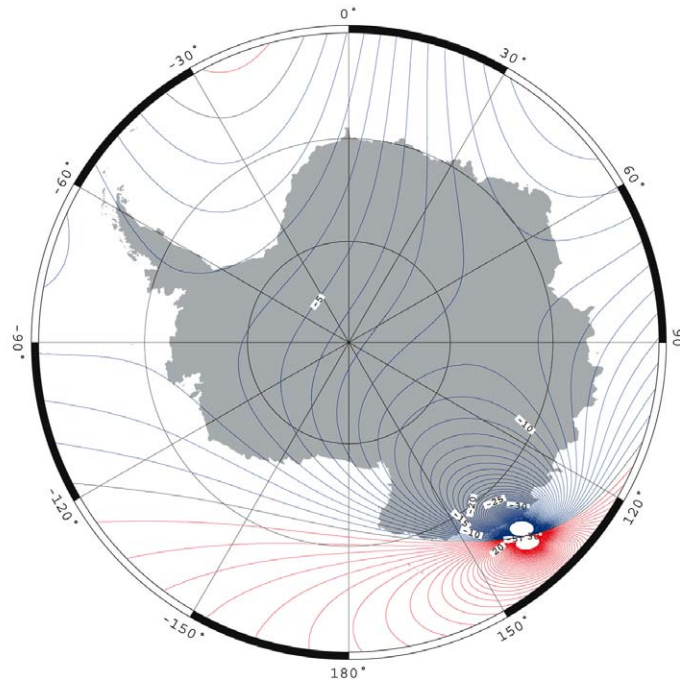
**Annual Rate of Change of Magnetic Vertical Intensity (Z)  
for 2005-2010 from the World Magnetic Model 2005**



North polar region, contour interval is 10 nT/year,  
red contours positive change; blue negative; black zero change.  
Polar Stereographic projection.

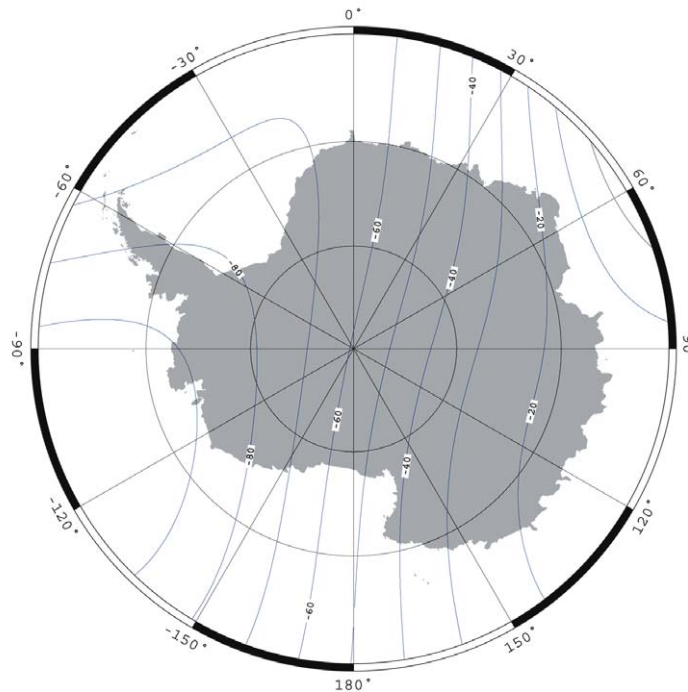
## Secular variation maps: South Polar Stereographic Projection

Annual Rate of Change of Magnetic Declination (D)  
for 2005-2010 from the World Magnetic Model 2005



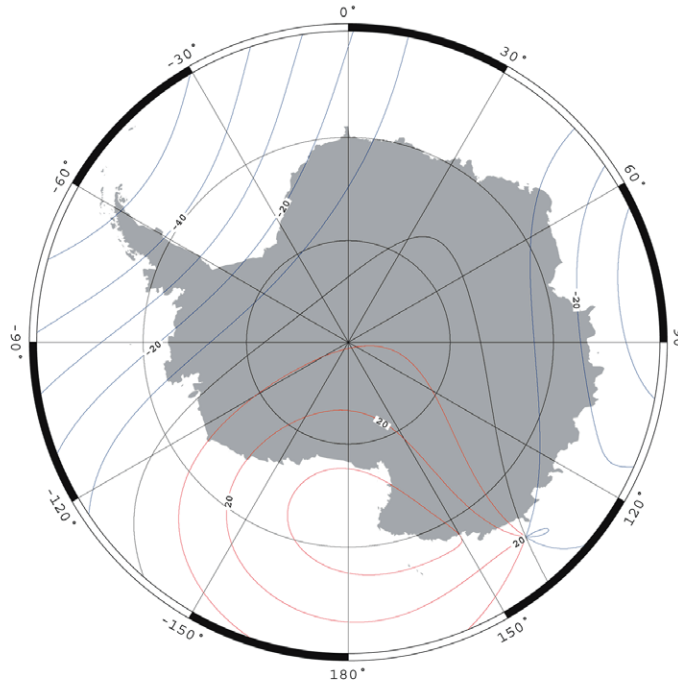
South polar region, contour interval is 1' / year up to 160' / year,  
red contours easterly change; blue westerly change;  
black zero change. Polar Stereographic projection.

Annual Rate of Change of Magnetic Total Intensity (F)  
for 2005-2010 from the World Magnetic Model 2005



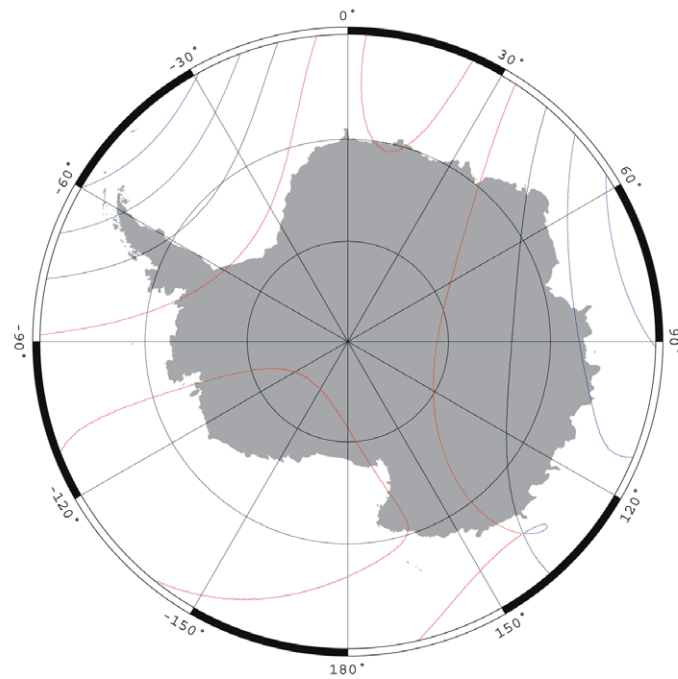
South polar region, contour interval is 10 nT/year.  
Polar Stereographic projection.

**Annual Rate of Change of Magnetic Horizontal Intensity (H)  
for 2005-2010 from the World Magnetic Model 2005**



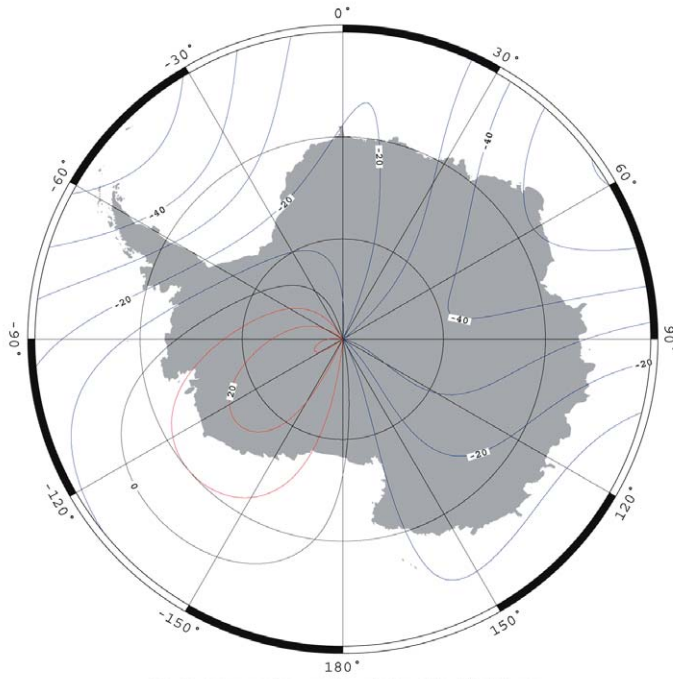
South polar region, contour interval is 10 nT / year,  
red contours positive change; blue negative; black zero  
change. Polar Stereographic projection.

**Annual Rate of Change of Magnetic Inclination (I)  
for 2005-2010 from the World Magnetic Model 2005**



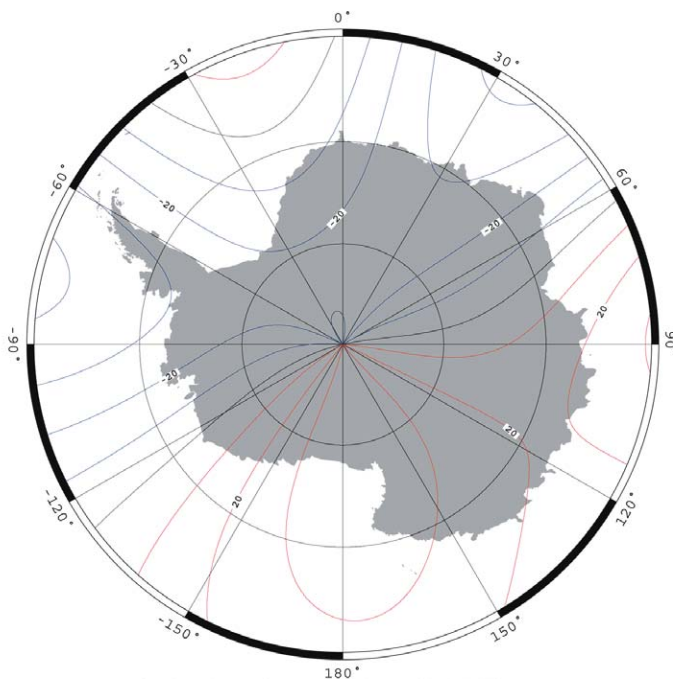
South polar region, contour interval is 1' / year,  
red contours positive change; blue negative; black zero change.  
Polar Stereographic projection.

**Annual Rate of Change of Magnetic North Component (X)  
for 2005-2010 from the World Magnetic Model 2005**



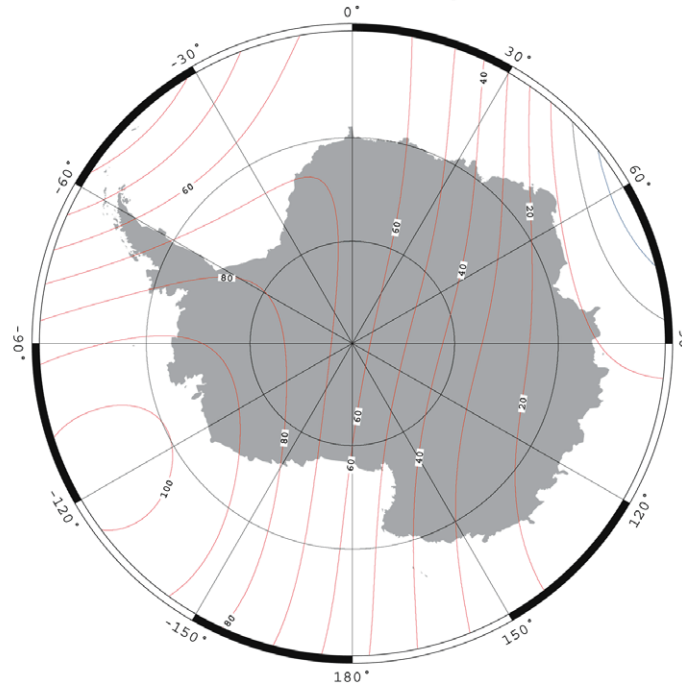
South polar region, contour interval is 10 nT/year,  
red contours positive change; blue negative; black zero change.  
Polar Stereographic projection.

**Annual Rate of Change of Magnetic East Component (Y)  
for 2005-2010 from the World Magnetic Model 2005**



South polar region, contour interval is 10 nT/year,  
red contours positive change; blue negative; black zero change.  
Polar Stereographic projection.

Annual Rate of Change of Magnetic Vertical Intensity (Z)  
for 2005-2010 from the World Magnetic Model 2005



South polar region, contour interval is 10 nT/year,  
red contours positive change; blue negative; black zero change.  
Polar Stereographic projection.

## References

Defense Mapping Agency, 1993. *Military specification for World Magnetic Model (WMM)*. Document MIL-W-89500.

Gradshteyn, I.S. and I.M. Ryzhik, 1994. *Table of integrals, series and products*, 5<sup>th</sup> ed., Academic Press.

Holme, R., 2000. Modelling of attitude error in vector magnetic data: application to Ørsted data. *Earth Planets and Space*, 52, 1187-1197.

Holme, R., N. Olsen, M. Rother, and H. Lühr, 2003. CO2 – A CHAMP magnetic field model, *First CHAMP Mission Results for Gravity, Magnetic and Atmospheric Studies*, edited by C. Reigber, H. Lühr, and P. Schwintzer, Springer, Berlin, 220–225.

Jankowski, J. and C. Sucksdorff, 1996. *Guide for magnetic measurements and observatory practice*. International Association of Geomagnetism and Aeronomy.

Kivelson, M.G. and C.T. Russell, 1995. *Introduction to space physics*. Cambridge University Press.

- Langel, R.A. and R.H Estes, 1985. Large-scale, Near-Earth magnetic fields from external sources and the corresponding induced internal field, *J. Geophys. Res.*, 90, 2487-2494.
- Langel, R.A. and W.J. Hinze, 1998. *The magnetic field of the earth's lithosphere: The satellite perspective*. Cambridge University Press.
- Lemoine, F.G., S.C. Kenyon, J.K. Factor, R.G. Trimmer, N.K. Pavlis, D.S. Chinn, C.M. Cox, S.M. Klosko, S.B. Luthcke, M.H. Torrence, Y.M. Wang, R.G. Williamson, E.C. Pavlis, R.H. Rapp and T.R. Olson., 1998, *The development of the joint NASA GSFC and the National Imagery and Mapping Agency (NIMA) geopotential model EGM96*. NASA/TP-1998-20681.
- Lesur, V., S. Macmillan, and A. Thomson, 2004. Magnetic field model with daily variations of the magnetospheric field and its induced counterpart in 2001. *Geophys. J. Int.*, doi: 10.1111/j.1365-246X.2004.02479.x.
- Lowes, F. J. and N. Olsen, 2004. A more realistic estimate of the variances and systematic errors in spherical harmonic geomagnetic field models. *Geophys. J. Int.*, 157, 1027-1044.
- Lühr, H., M. Rother, S. Maus, W. Mai, D. Cooke, 2003, The diamagnetic effect of the equatorial Appleton anomaly: Its characteristics and impact on geomagnetic field modelling *Geophys. Res. Lett.*, 30, n° 17, 10.1029/2003GL017407.
- Macmillan, S. and J.M. Quinn, 2000. The derivation of World Magnetic Model 2000. *British Geological Survey Technical Report WM/00/17R*.
- Macmillan, S. and J.M. Quinn, 2000. The 2000 revision of the joint UK/US geomagnetic field models and an IGRF2000 candidate model. *Earth, Planets and Space*, 52, 1149-1162.
- Maus, S. and Weidelt, P., 2004. Separating magnetospheric disturbance magnetic field into external and transient internal contributions using 1D conductivity model of the Earth. *Geophys. Res. Lett.*, 31, n° 12, L12614, 10.1029/2004GL020232.
- Maus, S. and A. Kuvshinov, 2004. Ocean tidal signals in observatory and satellite magnetic measurements, *Geophys. Res. Lett.*, 31, n° 15, L15313, 10.1029/2004GL020090.
- Merrill, R. T., M.W. McElhinny and P.L. McFadden, 1996. *The magnetic field of the earth*. Academic Press.
- Olsen, N., 2004. New parameterization of external and induced fields for geomagnetic field modeling. *Geophysical Research Abstracts* Volume 6. Abstracts of the Contributions of the EGU General Assembly, Nice, France, April 2004.
- Parkinson, W. D., 1983. *Introduction to geomagnetism*. Scottish Academic Press.

- Quinn, J. M. and S. Macmillan, 1999. The joint US/UK 2000 epoch World Magnetic Model and the GEOMAG/MAGVAR algorithm. Report and software.
- Sabaka, T.J., N. Olsen, and R.A. Langel, 2002. A comprehensive model of the quiet-time, near-Earth magnetic field: phase 3. *Geophys. J. Int.*, 151, 32-68.
- Sugiura, M., 1964. Hourly values of the equatorial Dst for the IGY, *Ann. IGY*, 35, 9–45.
- Tyler, R., S. Maus, and H. Lühr, 2003. Satellite observations of magnetic fields due to ocean tidal flow, *Science*, 299, 239-241.
- Utada H., H. Koyama, H. Shimizu, and A.D. Chave, 2003. A semi-global reference model for electrical conductivity in the mid-mantle beneath the north Pacific region. *GRL*, 30, 10.1029/2002GL016092.